Persistent effect of El Niño on global economic growth

Christopher W. Callahan[1,2*] & Justin S. Mankin[2,3,4]

[1]Program in Ecology, Evolution, Environment and Society, Dartmouth College, Hanover, NH
[2]Department of Geography, Dartmouth College, Hanover, NH
[3]Department of Earth Sciences, Dartmouth College, Hanover, NH
[4]Ocean and Climate Physics, Lamont-Doherty Earth Observatory of Columbia University, Palisades, NY
*Corresponding author, Christopher.W.Callahan.GR@dartmouth.edu

El Niño-Southern Oscillation (ENSO) shapes extreme weather globally, causing myriad socioeconomic impacts. But whether economies recover from ENSO events and how changes to ENSO from anthropogenic forcing will affect the global economy are unknown. Here we show that El Niño persistently reduces country-level economic growth, attributing $4.9T and $7.4T in global income losses to the 1982-83 and 1997-98 El Niños, respectively. Increases in ENSO amplitude and teleconnections from warming cause $374T in discounted global losses over the 21st century in a middle-of-the-road emissions scenario, but these effects are shaped by stochastic variation in the future sequence of El Niño and La Niña events. Our results highlight both the sensitivity of the economy to climate variability independent of warming and the possibility of future growth reductions due to anthropogenic intensification of such variability.

As the leading mode of interannual climate variability, El Niño/Southern Oscillation (ENSO) integrates a wide range of Earth system processes (*1*). El Niño events shift deep convection from the western to the eastern Pacific, reorganizing global atmospheric circulation and shaping remote weather through "teleconnection" patterns (*2*, *3*). The resulting temperature and hydroclimate extremes have many well-documented impacts, including flooding (*4*, *5*), crop losses (*6*, *7*), and civil conflict (*8*). Many climate models project that warming will increase El Niño amplitude (*9*, *10*) and frequency (*11*), with potentially devastating socioeconomic impacts (*12*).

Despite ENSO's global impacts, however, empirical climate-economy studies have generally focused on average temperature and rainfall (*13–18*) or daily-scale temperature variability (*19*), leaving open the possibility for unquantified costs from changes in dominant modes of climate variability. While studies have shown that El Niño reduces contemporaneous economic growth (*20–22*) and drives global commodity price fluctuations (*23–25*), it remains unclear if and for how long its economic impacts persist. Distinguishing between transient and persistent impacts on economic growth is essential. Transient impacts ("level effects") are quickly recovered, as an economy rebounds to its original trajectory. Persistent impacts ("growth effects") reduce an economy's ability to grow, compounding exponentially in time (*26–28*). Poor observational constraints on these growth effects limit our ability to understand the macroeconomic costs of ENSO and constrain this key uncertainty in climate damage projections (*26–28*).

Here we estimate the effect of ENSO on economic growth historically and in the future, accounting for the heterogeneity of ENSO teleconnections in space and time. We define ENSO by the E-index and C-index (*29*) (SM Fig. 1), metrics of El Niño and La Niña, respectively, that capture the nonlinear feedbacks that drive ENSO (Methods). We define country-level teleconnections for each index (τ^E and τ^C) using correlation coefficients between the winter E- and C-index and monthly country-level temperature and precipitation (Methods). Teleconnections are strongest in tropical countries and weaker in the midlatitudes (Fig. 1a), consistent with the physical responses of regional climate to tropical variability (*30*).

We use a distributed lag regression model to quantify the effect of ENSO on growth in national Gross Domestic Product per capita (GDPpc). Departing from previous work (*8*, *21*, *22*), we do not separate countries into teleconnected and non-teleconnected groups. Instead, we interact the E- and C-indices with teleconnections to allow the economic effect of ENSO to smoothly vary as a function of teleconnection strength (*31*) (Methods). The distributed lag model compares economic growth before and after El Niño events to assess the cumulative effects of these events over time, allowing us to distinguish growth from level effects (Methods). We focus on the five years following El Niño events, but also evaluate effects out to 15 years and for La Niña as well. We then couple these empirical estimates with projections of ENSO amplitude and teleconnections to assess the future economic effect of changes to ENSO.

El Niño persistently reduces growth

El Niño events persistently decrease economic growth (Fig. 1b). The magnitude of this effect is determined by the strength of each country's E-index teleconnection. In Peru ($\tau^E = 1.26$), for example, a 1-standard-deviation (s.d.) El Niño event decreases growth by 1.6 percentage points (p.p.) in the year of the event (95% confidence interval [CI]: 1.1 – 2.0 p.p.). Within five years, growth in a country as teleconnected as Peru declines by 7.1 p.p. (CI: 5.2 – 9.6) (Fig. 1b). By contrast, weakly teleconnected countries ($\tau^E < 0.5$) have small and uncertain effects (Fig. 1b). Interacting El Niño and teleconnections allows us to calculate marginal effects for each country based on their τ^E value (Fig. 1c). It also allows statistical significance to be determined by uncertainty in the distributed lag model itself (i.e., whether the 95% CI for a country includes zero; hatching in Fig. 1c), rather than an ex ante determination of "teleconnected" versus "non-teleconnected" countries. Some 56% of countries experience statistically significant declines in growth 5 years after an El Niño, averaging -2.3 p.p. per s.d. Critically, the increasing economic effect of El Niño with additional lags implies that these countries experience persistent growth reductions after an El Niño, not simply level effects from which they recover immediately (Fig. 1d). No countries experience significant benefits from El Niño.

The negative growth effects of El Niño are robust to alternative methodological choices, including using alternative growth data, excluding the most strongly teleconnected countries, using alternative teleconnection metrics, using more restrictive standard error clustering, using the Niño3 index instead of the E- and C-index, excluding the country fixed effect, and adding an annual total precipitation covariate (Methods, SM Figs. 2-4). Our model includes linear and nonlinear annual mean temperature terms to ensure that the effect of ENSO is not simply capturing the well-studied effect of mean temperature on growth (*13–15*, *17*). Removing these terms slightly increases the effect of El Niño, indicating that a small portion of ENSO's effect is due to its influence on mean temperatures (SM Fig. 2). Finally, accounting for country-specific growth trends does not strongly alter our results (Methods, SM Fig. 2), consistent with expectation since ENSO is stochastic on decadal timescales (*32*) and measured by a detrended index.

Distributed lag models that include additional lags yield similar results, with El Niño's effects persisting to 12 years or beyond (SM Fig. 5). Our focus on 5 lags reflects a balance between tracing the long-run response to ENSO and a concern for statistical power given the short observational record. Akaike Information Criterion values modestly decrease with increased lags, indicating better-fitting models, but the degrees of freedom also decrease (SM Fig. 5); using 5 lags balances these two criteria. When 15 or more lags are included, the model becomes unstable due to the large number of parameters being estimated (SM Fig. 5). Our interpretation of a permanent growth effect of El Niño is further bolstered by synthetic data simulations (Methods). These simulations use a perfect model framework where a permanent effect of El Niño is imputed to data to demonstrate that a model with many lags can yield insignificant and unstable coefficients due to the reduced sample size and large number of parameters being estimated, even if the effect is known and permanent (SM Fig. 5).

Our empirical model includes both the E-index and C-index, allowing us to estimate the effects of eastern Pacific El Niño (where El Niños are strongest) and the central Pacific La Niña (where La Niñas are strongest) (Methods). Central Pacific La Niña events have beneficial effects (SM Fig. 6), but they are several times weaker than the negative effects of eastern Pacific El Niño. The most strongly teleconnected countries experience a ~7.4-p.p. growth loss five years after an El Niño, but growth benefits of only ~1 p.p. five years after a La Niña. The C-index coefficients are also generally statistically insignificant under more restrictive standard error clustering, in contrast to the E-index (SM Tables 1 and 2). This result also implies that central Pacific El Niños, represented by positive C-index values, have weaker negative effects than eastern Pacific El Niños. These results reflect the skewness of ENSO, whereby eastern Pacific El Niños tend to be stronger than both La Niñas and central Pacific El Niños, and are consistent with previous studies showing that La Niña's economic effect is small (*21*, *22*).

El Niño's influence varies with income, with low-income countries suffering more damage than high-income countries (SM Fig. 2). The majority of highly teleconnected countries are lower-income, tropical countries (Fig. 1), extending previous work that identifies the strongest effect of El Niño in these countries (*21*). Importantly, however, high-income countries still experience statistically significant negative effects (SM Fig. 2), implying that wealth does not make economies invulnerable to El Niño. This finding is consistent with a broader literature showing that high-income countries are measurably impacted by extreme rainfall (*18*) and heat (*33*), both of which ENSO affects.

Our results are also similar across countries that experience wetting and drying in response to El Niño, with both experiencing persistent losses (SM Fig. 2), as both anomalously low and high rainfall can be economically damaging (*18*). More broadly, we emphasize that some regions can benefit from El Niño or be damaged by La Niña. Our goal in this work is to estimate a globally generalizable response to ENSO. That our findings are robust across multiple lines of country heterogeneity provides confidence that they are broadly generalizable, even though countries or regions within countries may respond differently.

Losses from historical El Niño events

The persistent effect of ENSO implies that historical El Niño events have permanently altered the income trajectories of teleconnected countries, potentially generating large economic losses. Here we quantify the costs of the two largest El Niño events in the last 60 years, the 1982-1983 event and the 1997-98 event (Fig. 2). Because an El Niño can trigger a subsequent La Niña (*34*), our analysis incorporates both the negative effects of each El Niño and the smaller benefits of the subsequent La Niña (Methods).

Consider Peru, among the most strongly teleconnected countries ($\tau^E = 1.26$). Its GDPpc declined in 1998 relative to 1997 and remained below the 1997 level for three more years, before rising again (Fig. 2a). Our empirical model suggest that Peru's economy would have grown much more quickly if the 1997-98 El Niño had not occurred (Methods). Income for the average Peruvian would have been some $1,753 greater five years later in 2003 (CI: $1,202 – $2,529), an increase of 27% (Fig. 2a). We find similar effects of this historic event across the tropics, with countries like Ecuador, Brazil, and Indonesia losing anywhere from 5% to 22% of their GDPpc due to the 1997-98 El Niño (SM Fig. 7).

These losses suggest large global costs of extreme El Niño events. Aggregating over all countries with statistically significant marginal effects (SM Fig. 7), global losses from the 1982-83 and 1997-98 events amount to trillion of dollars (Fig. 2b). The costs of the 1982-83 event began at ~$239B in 1983 but rose to more than $4.9T (CI: $3.1T – $6.7T) by 1988. Similarly, the costs of the 1997-98 event initially tallied some $455B but reached $7.4T (CI: $4.1T – $10.4T) by 2003. The greater costs of the 1997-98 event result both because it was a stronger El Niño event and because the global economy was larger. Absent the compensating benefits of the subsequent La Niñas, the 1983 event would have led to global economic losses of $5.3T, while the 1998 event would have cost $9.7T (Fig. 2b).

Our findings show very large and unaccounted-for economic losses from El Niño. Our estimates exceed previous ones; one study placed the total costs of the 1997-98 event at $36 billion, primarily in physical structures in low-income nations (*35*). By considering overall GDP, incorporating growth reductions in the years after the event, and including all countries in a single framework, our findings show that estimates that focus on physical asset losses in low-income countries alone have strongly underestimated the global economic toll of El Niño.

Climate model projections of ENSO

The growth effect of ENSO raises the question of how future changes to ENSO will affect the global economy. We use climate model simulations from the sixth phase of the Coupled Model Intercomparison Project (CMIP6) under four Shared Socioeconomic Pathway (SSP) experiments to analyze changes in ENSO due to global warming (Methods). We limit our analysis to simulations that realistically represent the skewness in eastern Pacific sea surface temperatures (Methods), totaling 239 selected simulations across the four scenarios.

CMIP6 models project increased 21st-century El Niño amplitude relative to the historical period (Fig. 3a). The median simulation sees amplitude increases of 0.05 – 0.18 s.d. across emissions scenarios, consistent with previous projections of stronger wind-ocean coupling in the eastern Pacific (*9*, *12*, *36*). In relative terms, these increases are between 5 and 20% of historical amplitude. El Niño amplitude increases are not strongly scenario-dependent, with the weakest increases occurring in both SSP1-2.6 and SSP5-8.5. One reason for this may be the strong influence of internal climate variability on forced ENSO changes (*36*–*38*). Realizations from any one model can vary widely given each model's representation of internal variability (Fig. 3a, lower lines). For example, amplitude changes range from -0.18 s.d. to +0.37 s.d. in the MIROC6 SSP2-4.5 realizations, -0.017 s.d. to +0.35 s.d. in the MIROC-ES2L SSP2-4.5 realizations, and +0.03 s.d. to +0.5 s.d. in the EC-Earth3 SSP2-4.5 realizations.

E-index teleconnections also increase with warming (Fig. 3b). Global mean teleconnections increase by 0.016 – 0.08 across scenarios, which corresponds to relative increases of 4 – 15%. This finding is consistent with a more energetic atmospheric response to El Niño (*39*, *40*), though ENSO-driven circulation changes are unpredictable and can dampen variability in some teleconnected regions (*41*). As with El Niño amplitude, internal variability can generate a wide range of teleconnection changes consistent with the same model structure and forcing (Fig. 3b, lower lines).

Independent of El Niño amplitude and teleconnections, simulations differ in their E-index time series. Due to the sensitivity of climate variability to initial conditions (*36*–*38*) and multidecadal modulation in ENSO strength (*42*, *43*), any given year yields a wide range of E-index values across models and scenarios (Fig. 3c, SM Fig. 8). For example, Figure 3c shows two SSP2-4.5 simulations with similar amplitude changes but different sequences of eastern Pacific El Niños and La Niñas. MIROC-ES2L r6i1p1f2 experiences strong El Niño events early in the 21st century, while CESM2-WACCM r3i1p1f1 is dominated by La Niña events from 2020-2040. Because ENSO permanently alters the trajectory of an economy, accumulated damages over any finite time period depend on the sequence of El Niños and La Niñas that occur. If a period begins with beneficial La Niña events, those benefits have more time to accumulate than the damages from El Niños. Crucially, because ENSO is asymmetric (i.e., El Niños are stronger than La Niñas), the long-run expectation from increased ENSO amplitude is net economic losses.

We combine these projections with our empirical estimates to quantify the economic effects of changes in ENSO. We use the SSP scenarios as baselines and calculate country-level growth changes relative to this baseline if ENSO amplitude and teleconnections change as projected (Methods).

Economic impacts of future ENSO changes

Anthropogenic changes to El Niño amplitude and teleconnections may cause substantial economic losses over the 21st century (Fig. 4). Under a 2% discount rate (*44*) and a realistic emissions trajectory (*45*) (SSP2-4.5), the median cumulative 2020-2099 global losses are \$374T (Fig. 4a), a ~4% reduction in global economic output over the 21st century. Median losses exceed \$75T in all four emissions scenarios. Damages in all four scenarios are distinctly negatively skewed, consistent with the underlying asymmetry and nonlinearity in ENSO itself.

Uncertainty in the precise magnitude of these projected losses is large. Under SSP2-4.5, the 95% range spans losses of \$1909T to benefits of \$545T (we write this CI as -\$1909T – +\$545T) across 86,000 combinations of 86 simulations and 1,000 regression bootstraps (Fig. 4a). Reducing the discount rate to 1% amplifies median losses under SSP2-4.5 to \$654T (-\$3230T – +\$894T), while increasing it to 5% diminishes losses to \$82T (-\$485T – +\$154T). The most extreme end of these ranges corresponds to a ~20% reduction in global economic output over the remaining century. In highly teleconnected countries, global warming-induced changes to ENSO are associated with GDPpc reductions of >4% per year, though uncertainty is high even in these severely affected countries (SM Fig. 7c, d).

The principal reason for the substantial uncertainty in ENSO-driven losses is that the largely stochastic sequence of El Niños and La Niñas the world experiences going forward can shape the direction and magnitude of damages (Fig. 4b). For example, MIROC-ES2L r6i1p1f2 and CESM2-WACCM r3i1p1f1 have similar amplitude changes (+0.16 vs. +0.17). But MIROC-ES2L r6i1p1f2 has several extreme El Niño events early in the 21st century, while CESM2-WACCM r3i1p1f1 has beneficial eastern Pacific La Niñas over the same period (Fig. 3b). Under similar amplitude changes, MIROC-ES2L's E-index sequence implies losses of \$1756T (CI: -\$2326T – -\$1314T), while CESM2-WACCM's yields global benefits of \$1538T (CI: +\$1047T – +\$2302T). Critically, the combination of ENSO's persistent effects *and* its future time series creates this effect; if the effects of ENSO were recovered rapidly, El Niño events in the early 21st century would not influence end-of-century economic losses. We note that the sequence of individual events is not entirely stochastic—ENSO oscillates between El Niño and La Niña as driven by underlying physics—but multidecadal periods of strong or weak ENSO can arise stochastically and are often unpredictable (*42*).

Because we focus on the E-index, the sequence of El Niños and La Niñas described above refers to eastern Pacific events. However, beneficial La Niñas are most appropriately represented by the C-index, and could potentially offset some of the costs of El Niño. However, the economic effects of C-index changes are relatively small, and when added to the effects of E-index changes, overall damages are similar to E-index damages alone (SM Fig. 9a, b). As such, society should not rely on the benefits of La Niña to reduce the costs of changes to ENSO.

Using only one realization from each model increases uncertainty in damages across scenarios (SM Fig. 9c), suggesting the importance of large ensembles of climate simulations to capture the scope of ENSO variability under climate change (*37*). Alternative analytical choices, such as holding teleconnections constant or changing the start year for damages accumulation, does not change the core result of negative and skewed ENSO-driven damages with warming (SM Fig. 9d, e).

Despite the large uncertainties, the fact that these damages are broadly negative implies that increases in ENSO amplitude and teleconnections produce net economic losses. To formalize and decompose the contributions of amplitude and teleconnection changes while accounting for the ENSO time series realization, we use a multiple regression that relates variation in these factors to variation in damages across all climate model realizations (Methods). We summarize the "El Niño-ness" of the ENSO time series with the sum of the E-index over 2020-2069 (inset text, Fig. 3c), which we find to be a skillful predictor of initial ENSO strength (SM Table 3). We interact this metric with changes in ENSO amplitude and teleconnections for each simulation, allowing their effects to be modulated by the sequence of simulated ENSO events. This approach allows us to derive generalizable economic effects of forced changes in amplitude and teleconnections, particularly given that the unique ENSO sequence—though a major source of uncertainty in projected damages—is independent of forcing (SM Fig. 8).

Across simulations and scenarios, each 0.1-s.d. increase in ENSO amplitude causes cumulative global economic losses of $60T ($p < 0.001$, Fig. 4c, SM Table 3). Similarly, each 0.1-unit increase in ENSO teleconnections causes global economic losses of $315T ($p < 0.001$, Fig. 4d, SM Table 3). These numbers correspond to a 2% discount rate; increasing the discount rate reduces the magnitude and uncertainty of these estimates (Fig. 4c, d, left blue bars). These results build upon previous projections of changes in ENSO amplitude (*9*, *11*) and teleconnections (*39*, *40*), demonstrating tangible, global socioeconomic effects of these physical changes.

The responses shown in Fig. 4c and 4d are conditional on experiencing the average E-index time series across simulations, but there are also strong interactions between the time series and the effect of amplitude or teleconnection changes ($p < 0.01$). Consistent with the above discussion, a future with more El Niño events than average makes amplitude increases substantially more damaging, while one with more La Niña events than average reduces the resulting damages or even provides benefits (SM Table 3). The same is true for teleconnection changes.

Our findings have implications for both climate mitigation and adaptation. All else being equal, increases in ENSO amplitude and teleconnections due to global warming will generate major economic losses not currently included in assessments of climate damages and, therefore, in the assessment of mitigation benefits. However, the facts that (1) ENSO-driven damages do not depend strongly on future climate scenario (Fig. 4a) and (2) a wide range of negative or positive outcomes are possible due to uncertainty in the unique ENSO sequence the world experiences going forward (Fig. 4b) together imply that climate mitigation alone is insufficient to protect economies from El Niño's impacts. While emissions reductions remain the most effective means to blunt the economically catastrophic impacts of anthropogenic warming (*46*), our findings simultaneously raise the priority of climate adaptation and resilience efforts. Improved disaster risk management could reduce ENSO-driven damages by making economies more resilient to their devastating impacts (*47*). Moreover, scientific investments in ENSO prediction, decadal climate prediction, and climate variability could reduce the uncertainty in estimates of future ENSO-driven damages and better inform investments in climate resilience.

Conclusion

Our finding that El Niño has a persistent effect on economic growth has four key implications. Firstly, it demonstrates that, even independent of global warming, economic growth is more sensitive to climate variability than previously understood. The permanent impacts we identify extend previous work on the impacts of El Niño and demonstrate that the local extreme conditions associated with ENSO integrate into a globally persistent macroeconomic effect. This temporal persistence implies large and previously underestimated costs of historical El Niño events. Moreover, the sensitivity of economic growth to climate variability implies more severe losses from warming than previously assumed by some climate-economy models (*26*–*28*). Secondly, our results demonstrate that future changes to ENSO may increase the global macroeconomic costs of warming. Previous climate-economy studies have not incorporated changes in modes of climate variability, and we show that this omission has potentially hidden a major cost of rising temperatures. Thirdly, stochastic variation in ENSO could result in either losses or benefits from warming even in the face of enhanced ENSO amplitude, emphasizing the importance of investing in better ENSO prediction, particularly on decadal time scales (*42*). Lastly, these findings together suggest that while climate mitigation is essential to reducing the vulnerability of global economic growth to climate extremes, it remains imperative to devote substantially more resources to adapting to El Niño events in the present day.

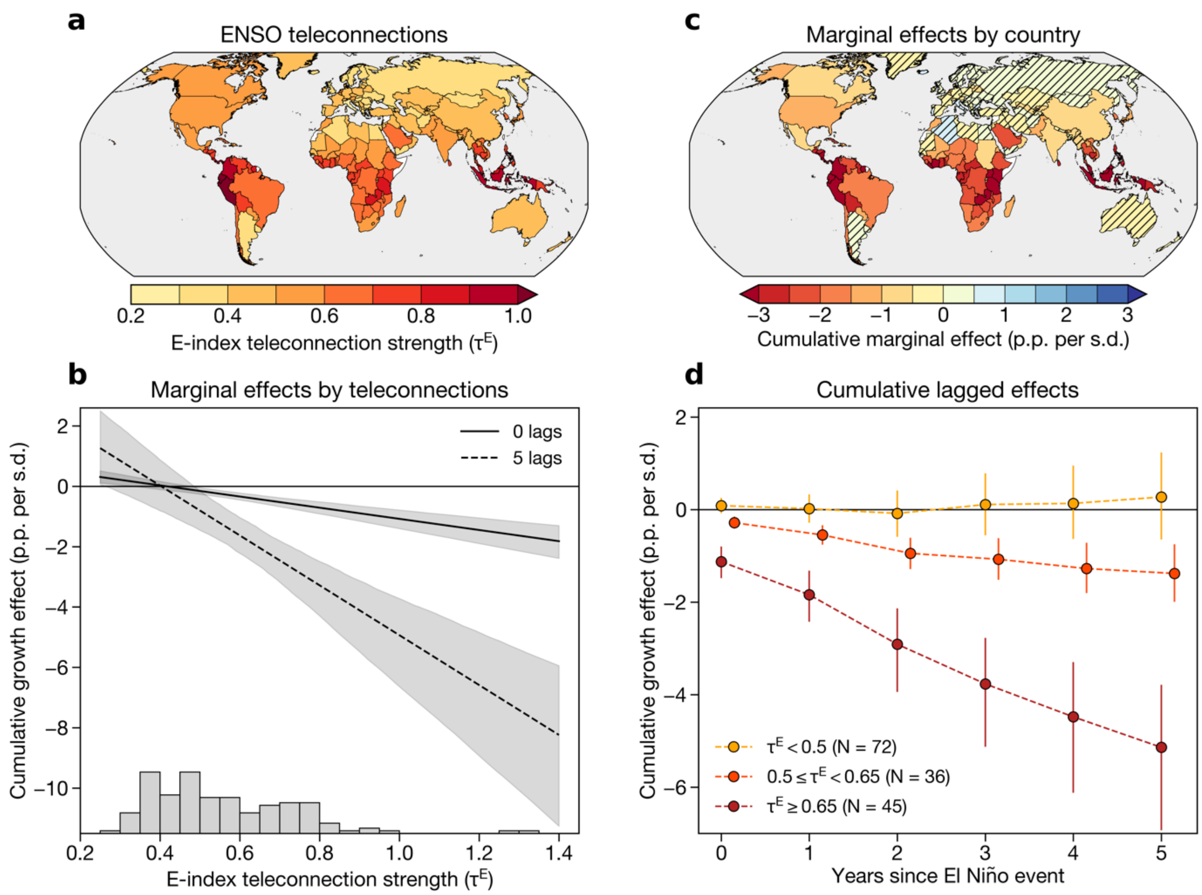

Fig. 1 | Teleconnections mediate the effect of El Niño on economic growth. A) Country-level ENSO teleconnections, calculated as the sum of the absolute value of the correlation coefficients between the E-index and monthly country-level temperature and precipitation (Methods). **B)** Marginal effects of El Niño on economic growth across teleconnection values in year of the event (0 lags, solid line) and the fifth year after the event (5 lags, dashed line). Black line shows the mean and shading shows 95% confidence intervals from bootstrap resampling (Methods). Lower histogram shows the density of teleconnection values in the sample. **C)** Cumulative 5-lag effect of El Niño on economic growth for each country. Hatching denotes countries whose effects are not distinguishable from zero (i.e., they fall on a location on the x-axis in (B) where the shading includes zero). **D)** Cumulative effects of El Niño over time, beginning with the year of the event (year 0) and accumulating to the fifth year after the event (year 5). Countries are grouped into three bins according to their teleconnection strength, with "N" denoting the number of countries in each bin. Dots show averages and bars show 95% confidence intervals.

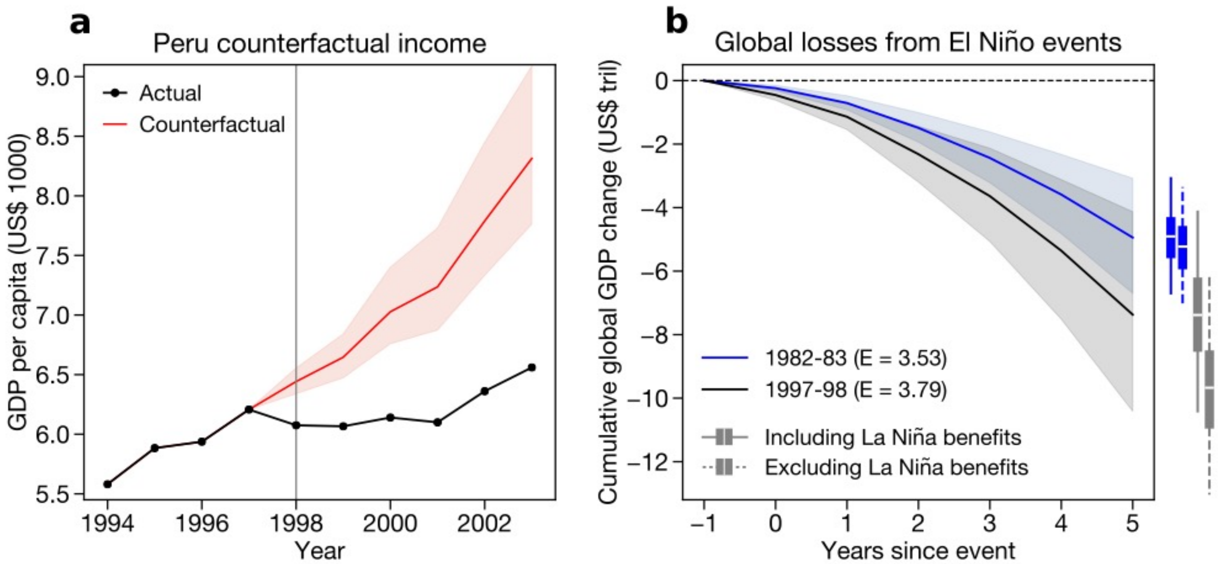

Fig. 2 | Damages from extreme El Niño events. A) GDP per capita (GDPpc) in Peru before and after the 1997-98 El Niño event. Black line shows actual GDPpc, red line shows the average counterfactual GDPpc across regression bootstrap samples (Methods), and red shading shows 95% confidence interval. **B)** Cumulative global GDP change for the 5 years after the 1982-83 (blue) and 1997-98 (black) El Niño events. Center line shows the mean and shading shows the 95% confidence intervals across regression bootstrap samples. Global GDP change is only calculated for countries with statistically significant marginal effects (Fig. 1c). Text in legends denotes the DJF-average E-index in the corresponding years. Boxplots at right show cumulative global GDP change when including the benefits of the following La Niña events (solid lines) and excluding those benefits (dashed lines). All dollar values are in constant 2017 prices.

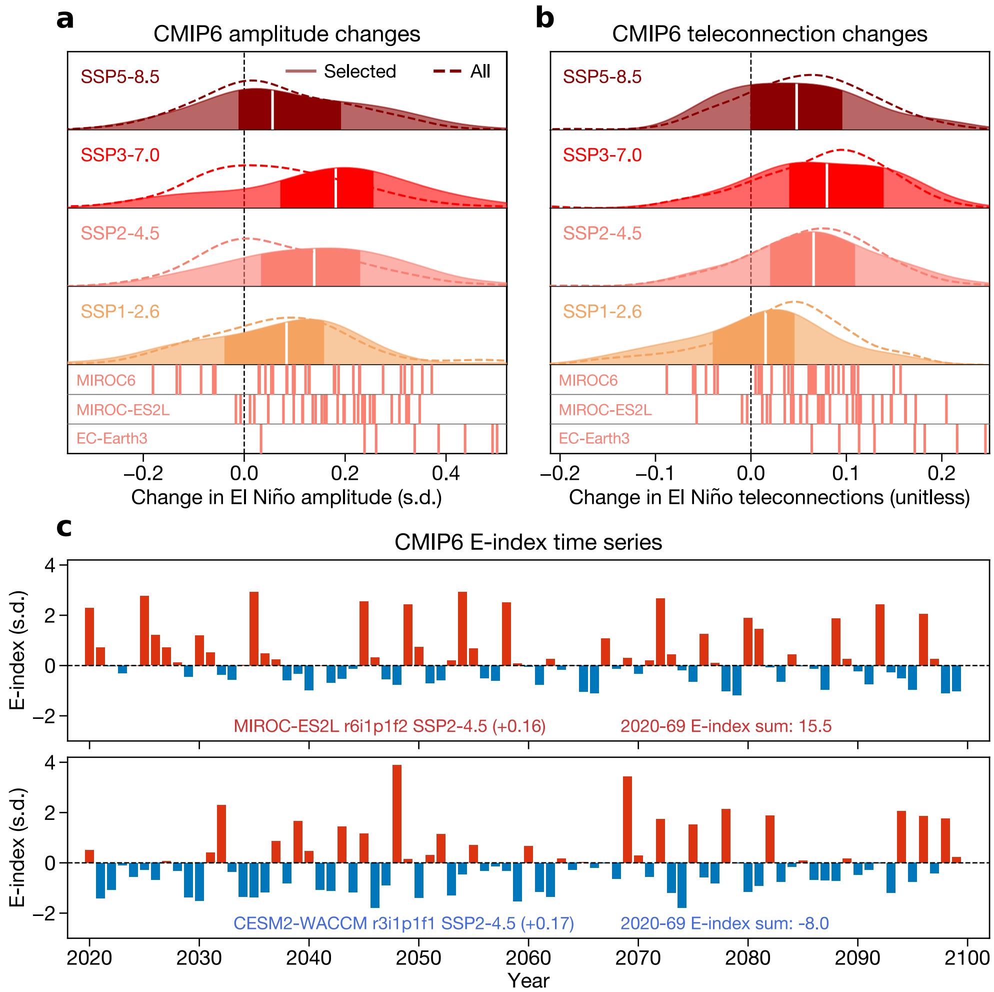

Fig. 3 | Climate model projections of ENSO. Change in ENSO amplitude (**A**) and global mean teleconnections (**B**) between 1940-2019 and 2020-2099 for an ensemble of CMIP6 simulations from four SSP experiments. In both panels, dashed density lines show changes from all simulations and solid density plots show amplitude changes from selected high-skill simulations used in the analysis (Methods). Vertical lines below density plots denote amplitude changes from the individual realizations of three models (MIROC6, MIROC-ES2L, and EC-Earth3), all drawn from the SSP2-4.5 experiment, illustrating the wide range of amplitude and teleconnection changes possible from internal variability alone. **C)** E-index time series from two example simulations with similar amplitude increases: MIROC-ES2L r6i1p1f2 (top) and CESM2-WACCM r3i1p1f1 (bottom), both from the SSP2-4.5 experiment. Red bars denote eastern Pacific El Niño (E > 0) and blue bars denote eastern Pacific La Niña (E < 0). Left inset text in each panel denotes the model information and amplitude change. Right inset text denotes the sum of each E-index time series between 2020-2069, with positive values indicating that the time series contains more El Niños than La Niñas and negative values indicating the opposite.

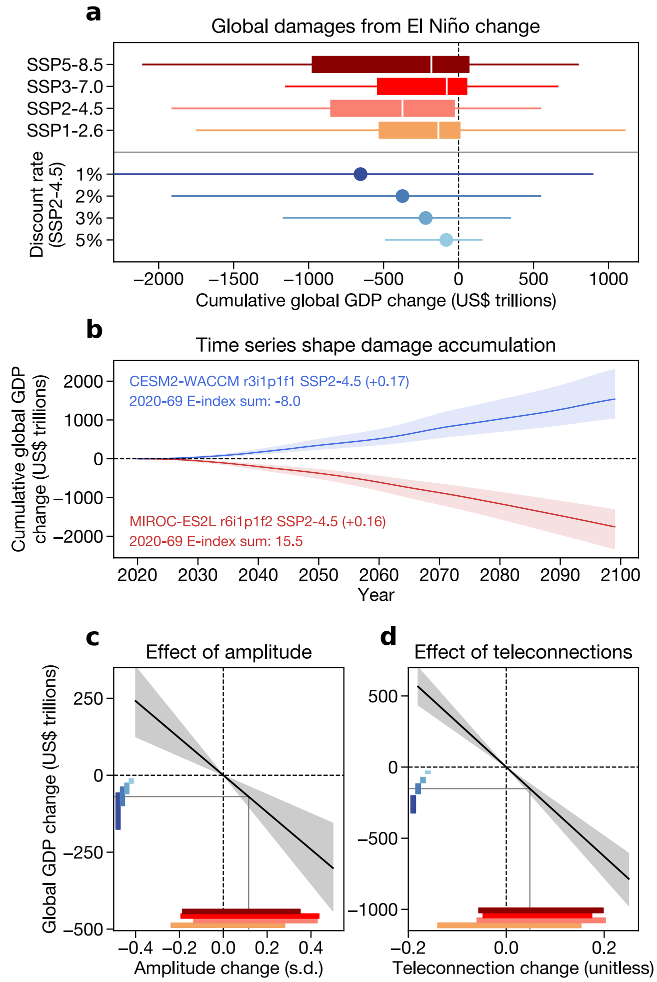

Fig. 4 | Global economic impacts of changes in El Niño amplitude and teleconnections. A) Boxplots show the cumulative global GDP change in each scenario under a 2% constant discount rate. Colors correspond to the scenario colors in Fig. 3. In each boxplot, white line denotes the median, box spans the first and third quartiles, and whiskers span the 95% range. Lower blue lines denote global economic losses under SSP2-4.5 and a range of discount rates. Dot denotes the median and lines span the 95% range. **B)** Cumulative global GDP change over time from two example SSP2-4.5 simulations with similar amplitude changes but different time series realizations (see Fig. 3c). Solid line denotes the median and shading shows the 95% range across regression bootstrap samples. **C, D)** Cumulative global GDP change due to changes in ENSO amplitude (**C**) and teleconnections (**D**) with a 2% discount rate. Solid black lines denote the regression estimate and shading shows the 95% CI from an inter-simulation multiple regression (Methods). Lower red lines show the 95% range of amplitude (**C**) or teleconnection (**D**) changes in each scenario. Thin gray lines denote the median change in amplitude (**C**) or teleconnections (**D**) across simulations and scenarios. Blue bars at left illustrate how the discount rates from (**A**) influence the 95% range of outcomes at the median change in amplitude or teleconnections (vertical gray lines).

SUPPLEMENTARY MATERIAL

Persistent effect of El Niño on global economic growth

Materials and Methods

Data

We use observational climate data from multiple sources: Monthly mean sea surface temperatures (SST) averaged across the ERSST (*48*) and HadISST (*49*) datasets, monthly mean atmospheric temperatures averaged across the Berkeley Earth (*50*), University of Delaware (*51*), and 20th Century Reanalysis (*52*) datasets, and monthly total precipitation data from the Global Precipitation Climatology Center (*53*). These datasets are averaged together to reduce observational uncertainty from any one gridded data product (*54–56*). Temperature and precipitation are aggregated to population-weighted country-level means using year-2000 population data from the Gridded Population of the World (*57*). We use population weighting to ensure that the spatial aggregation captures climate fluctuations that affect people and economic activity.

We use country-level economic data from the Penn World Tables version 10.0 (*58*), specifically Gross Domestic Product ("RGDPNA") (in 2017 dollars) and population ("POP") for all countries of the world. GDP per capita (GDPpc) is calculated as GDP divided by population. Growth for each year is calculated as the fractional GDPpc change relative to the previous year. Because macroeconomic data may contain measurement error (*59*), we also repeat the analysis using GDPpc data from the World Bank World Development Indicators (*60*), finding similar results (SM Fig. 2).

The time period of analysis for both the teleconnection calculations and regression analysis is 1960-2016, so all observational economic and climate data is limited to that time period.

Climate model data come from the sixth phase of the Climate Model Intercomparison Project(*61*) (CMIP6). We use monthly SST, monthly atmospheric temperature, and daily precipitation data over 1850-2099 from the historical experiment and the four Tier 1 experiments from the Scenario Model Intercomparison Project (*62*). These four experiments—SSP1-2.6, SSP2-4.5, SSP3-7.0, and SSP5-8.5—span a range of plausible policy futures, from aggressive mitigation (SSP1-2.6) to high emissions (SSP5-8.5) (*62*, *63*). Global mean temperatures rise by ~1.2 °C by 2081-2100 relative to 1995-2014 in the SSP1-2.6 scenario, 2.1 °C in SSP2-4.5, 3.2 °C in SSP3-7.0, and 4 °C in SSP5-8.5 (*63*). Not all models have data available for each experiment, so differences across the experiments are due both to differences in forcing and differences in the sampling of model structure (SM Tables 4-7).

The temperature data is regridded to the Berkeley Earth 1°-by-1° grid, the HadISST data is regridded to the ERSST 2°-by-2° grid, and all climate model data is regridded to a 2°-by-2° grid, using bilinear interpolation from Python's "xarray" package (*64*).

ENSO indices

We use the "E-index" and "C-index" to represent ENSO (*9*, *29*, *36*, *65*, *66*). The E-index represents eastern Pacific El Niño events and captures the nonlinear processes that generate positive skewness in eastern Pacific SSTs, whereby El Niño events are stronger than La Niña events (*9*, *29*). The E-index is a combination of the first two principal components (PCs) of an empirical orthogonal function (EOF) analysis applied to Pacific SSTs (*36*) over 20 °S – 20 °N and 140 °E – 80 °W, specifically as $E = (PC1 - PC2)/\sqrt{2}$. We calculate the E-index in observations using linearly detrended SST anomalies referenced to 1960-2016 long-term monthly means. We then average the E-index over winter (December-February, DJF), to focus on the season in which ENSO peaks (*67*); the E-index in year *t* is therefore defined as the average of the December E-index from year *t-1* and the January and February indices from year *t*.

The C-index (*29*) is a companion index to the E-index and is calculated as $C = (PC1 + PC2)/\sqrt{2}$. The C-index represents central Pacific La Niña and El Niño events, where La Niña events tend to be stronger than El Niño events. Positive E-index values represent an eastern Pacific El Niño event and negative C-index values represent a central Pacific La Niña event. The E-index and C-index are orthogonal by construction (*29*), allowing us to include them both in a regression model without a concern for collinearity.

To assess the sensitivity of our results to these indices, we also calculate the Niño3 index, defined as linearly detrended SST anomalies averaged over 5 °S – 5 °N and 150 °W – 90 °W. The Niño3 index yields similar, though slightly weaker, results to the E-index (SM Fig. 2) since it corresponds to eastern Pacific conditions.

We calculate the DJF E- and C-index similarly in the CMIP6 models, using quadratically detrended (*9*) SST anomalies referenced to monthly means from 1850-2014.

Country-level ENSO teleconnections

Our analysis incorporates a country-specific teleconnection metric to quantify heterogeneity in growth responses according to a country's geophysical connection to ENSO. To calculate the teleconnection, we first standardize monthly country-level mean temperature and total precipitation by subtracting the long-term (1960-2016) monthly mean and dividing by the long-term monthly standard deviation. We then linearly detrend these standardized anomalies separately for each month to remove the effects of warming and low-frequency climate variability.

Next, we correlate these standardized temperature and precipitation time series with the DJF E-index separately for each month *m* and each country *i.* El Niño events begin and grow in year *t-1*, peak in the winter, and then decay in the spring and summer of year *t*, so we allow the DJF E-index to affect both the preceding (beginning just after the “spring predictability barrier” in June of *t-1*) and following years (ending in August of year *t*) (SM Fig. 1). We use partial correlations to control for precipitation when analyzing temperature and vice versa to control for the covariance between temperature and precipitation.

This calculation yields a distribution of 15 correlation coefficients (one per month from June of year *t-1* through August of year *t*) for each country, separately for temperature and precipitation. We then take the three-month running mean of these coefficients across the 15 months to smooth out random variation and account for multiple months of exposure to ENSO. Finally, we take the maximum (absolute) correlation coefficients from these running means for both temperature and precipitation and add them together to calculate each country’s E-index teleconnection τ^E. We use absolute values to allow the distinct effects of temperature and precipitation teleconnections to be additive, but our results are robust to considering both positive and negative precipitation teleconnections separately (SM Fig. 2).

This teleconnection metric estimates the degree to which each country’s climate is influenced by ENSO, accounting for: (1) the effects of both temperature and precipitation; (2) multiple sustained months of exposure to ENSO; and (3) the varied timescales on which country-level teleconnections may manifest. Additionally, this strategy allows teleconnections to be defined continuously rather than separating teleconnected and non-teleconnected countries based on arbitrary significance thresholds (*8*) or relying on previously defined climate zones (*21*, *22*). We perform the same analysis with the C-index to calculate C-index teleconnections (τ^C).

Our main analysis uses a correlation coefficient to calculate teleconnections, but we also assess the sensitivity of this choice by using partial regression coefficients instead. Using a regression coefficient leads Peru and Ecuador to be strong outliers from the rest of the distribution (SM Fig. 2e), with τ^E values at or above 2. Estimating the growth regression with these values leads to large uncertainties as Peru and Ecuador have an outsized influence on the regression (SM Fig. 2e), so the correlation coefficient is a more stable metric for use in the growth regression. However, we emphasize that the effect of El Niño is still strong and statistically significant when using regression coefficients, so our results are not an artifact of the choice to use the correlation coefficient.

We can also define teleconnections solely based on the temperature or precipitation portions of the calculation, similar to previous studies that have focused on temperature to define teleconnections (*6*, *8*). Results for this sensitivity analysis are shown in SM Fig. 4. The temperature-based estimate is similar to that from both temperature and precipitation, but the effect is weaker with precipitation alone. Our interpretation is that aggregating the data to the monthly time scale and country spatial scale dampens the signal of precipitation more than it does temperature. Consistent with this interpretation, empirical climate-economy studies tend to find little effect of precipitation on country-level growth (*13*, *17*).

Additionally, by using the maximum of three-month running means, our analysis focuses on countries' short-term extreme exposure to ENSO rather than capturing cumulative exposure over the entire ENSO life cycle. An alternative teleconnection metric which uses the sum of statistically significant ($p < 0.05$) correlation coefficients across the 15 months for each country yields very similar results, with high correlations between this and our original metric and nearly identical marginal growth effects (SM Fig. 4). This analysis implies that focusing on the few months of maximum exposure is sufficient to capture the effects of ENSO on economies broadly.

Our main analysis treats teleconnections as constant in time in the observational period. However, sampling variability and changes in ENSO behavior (among other things) may result in temporal heterogeneity in teleconnections. SM Fig. 10 shows teleconnections calculated in rolling 30-windows over the historical period. Temporal variation is apparent, at least partly due to the shorter time period used to calculate these teleconnections. However, the distribution of teleconnection values is relatively stable, and the average country experiences temporal variation of only about 13% of its mean value. As such, we use the teleconnection values calculated across the entire time period in our main analysis. We do allow teleconnections to change with forcing in our climate model analysis (as described below).

Additionally, a key consideration in empirical climate-economy studies is the need to aggregate physical variables to the country scale, which is not a geophysically meaningful scale. As such, we re-calculate E-index teleconnections at the gridded scale (SM Fig. 10). Teleconnections can vary across grid cells (SM Fig. 10c), but the average country only experiences within-country spatial variation of about 11% of its mean teleconnection value (SM Fig. 10e). Furthermore, population-weighted country-average grid-cell teleconnection values are similar to the original teleconnection values calculated from country-average temperature and precipitation (SM Fig. 10f), implying that subnational spatial variation in the strength of ENSO teleconnections does not substantially affect our results.

Econometric analysis

The goal of our analysis is to quantify the multi-year effect of ENSO on economic growth. This task requires us to separate ENSO from the other constant and time-varying factors that affect economic growth. We use a distributed lag regression model, estimated with Ordinary Least Squares, to estimate the effects of eastern Pacific El Niño (the E-index) and central Pacific La Niña (the C-index) on growth:

$$g_{it} = \sum_{L=0}^{j} \left[\beta_L E_{t-L} + \Theta_L E_{t-L} * \tau_i^E + \Phi_L C_{t-L} + \Psi_L C_{t-L} * \tau_i^C + \alpha_L T_{i(t-L)} + \gamma_L T_{i(t-L)}^2 \right] + \mu_i + \epsilon_{it} \qquad (1)$$

Here, g refers to growth in country *i* in time *t*, E refers to the E-index in year *t*, C refers to the C-index in year *t*, and T refers to annual mean temperature. μ is a country fixed effect, which controls for average differences between countries such as geography and ensures that our results are identified using within-country variation in growth. We include the mean temperature terms to ensure that the effect of ENSO is independent of the well-studied effect of mean temperature on economic growth. Finally, the interactions of E with τ^E and C with τ^C allow the effect of ENSO to differ between countries based on how strongly coupled each country's climate is to ENSO.

The identifying assumption for Eqn. 1 is that E is as-good-as-randomly-assigned with respect to growth. Because the E-index describes the physical structure of SST anomalies in the Pacific, it is plausibly exogenous from the other factors that affect growth. The E-index is constant across countries within each year, so the identifying variation comes from stochastic and unpredictable (*32*, *68*) shifts in SSTs from year to year. The E-index is not highly correlated with itself across lag lengths (SM Table 8), meaning that including multiple lags in a single model should not generate multicollinearity.

The inclusion of lagged terms from years *L* to *j* is necessary to distinguish between level and growth effects on the economy. If the effect of El Niño only falls on income levels, then a shock in year *t* will be recovered in year *t+1* as countries rebound to their original income trajectory, meaning that year *t+1* will see an abnormally high growth rate. If, instead, El Niño affects the underlying capacity of the economy to grow, then the years following an event should show either persistent declines in growth or no change. As such, our analysis focuses on the cumulative coefficients Ω, which represent the accumulated effect of ENSO in the years after an event. The interaction of E with country-specific teleconnections τ allows us to calculate unique cumulative effects for each country *i* and lag length *L*:

$$\Theta_{iL} = \sum_{L=0}^{j}\left[\beta_L + \Theta_L * \tau_i^E\right] \tag{2}$$

If Ω_{iL} is indistinguishable from zero, then we cannot reject the hypothesis that El Niño has only level effects; growth effects are identified if Ω_{iL} is significantly different from zero ($p < 0.05$).

We estimate confidence intervals by bootstrapping (N = 1,000), with countries resampled from a uniform distribution with replacement. Countries are sampled as a block to account for within-country autocorrelation (*69*). However, alternative bootstrapping schemes yield similar results, such as sampling by year globally or within continents to account for spatial correlation in growth, sampling by continent to account for simultaneous spatial and temporal correlation, and sampling by five-year blocks to account for spatial and short-term temporal correlation (*69*) (SM Fig. 3). Multiple forms of clustered parametric standard errors, which are robust to both spatiotemporal autocorrelation in errors and heteroskedasticity across clusters, do not reduce the statistical significance of our results (SM Table 2).

We remove growth values from our sample that are above 18% or below -18%, approximately the 3σ range. We drop 138 values because of this choice, less than 2% of the sample. Including these values does not reduce the average effect, but it does increase the uncertainty (SM Fig. 2), so we drop these outliers while noting that our results would be similar if we included them.

The identifying variation in our model comes from year-to-year variation in ENSO, rather than spatial variation, raising the concern that ENSO could be correlated with other time-varying factors that affect growth. However, ENSO indices are detrended by construction and unlikely to be correlated with long-term trends in technology or productivity. To further explore this question, we estimate the model after adding country-specific linear growth trends to remove smoothly time-varying factors, yielding similar results to our main model (SM Fig. 2). Other work has used a combination of linear and quadratic trends (*13*); in our case, using both types of trends yields slightly weaker but still strong and statistically significant responses. Bootstrap resampling by year, which permutes the years in the regression to ensure that no single year drives the results, also yields similar results (SM Fig. 3). These results give us confidence that the effect of ENSO we find is not spurious.

When we estimate separate responses for high-income and low-income countries (SM Fig. 2c), we use the World Bank's income classifications, grouping low and lower-middle income countries together as well as high and higher-middle income countries.

Other time series analysis tools have been used to assess the effect of ENSO such as vector autoregression (VAR) models (*20*, *23–25*) or local projections (*20*). We use a distributed lag (DL) model for two reasons. Firstly, DL models have been widely used in the empirical climate-economy literature (*13*, *15*, *70*, *71*), so our approach is consistent with this work. Secondly, VAR models are primarily used in macroeconomic settings where endogeneity is at issue (*72*). Because ENSO is plausibly exogeneous to country-level growth rates, we adopt the more parsimonious DL model.

Synthetic data simulations

Estimating the effect of El Niño with models that include 15 or more lags results in unstable coefficients and confidence intervals that include zero (SM Fig. 5). Two plausible interpretations of this result are: (1) that there is no statistically significant growth effect of El Niño after 15 years; or (2) that there is a permanent growth effect, but models with many lags cannot confidently identify this effect due to the reduced sample size and increased number of parameters being estimated simultaneously.

To examine this issue, we use a perfect model framework where we impute a known El Niño effect to synthetic growth data and then estimate the regression on that data to assess whether we can recover the effect. We construct growth as the combination of a first-order autocorrelated process (AR(1)) with Gaussian noise of mean 0 and s.d. 0.05, a linear trend randomly chosen from a Gaussian distribution of mean 0 and s.d. 0.2 (in p.p. per year), and an El Niño effect. The AR(1) coefficient is set to 0.1, within the range of AR(1) coefficients from the data, and the distribution of trends we choose from is also similar to the distribution of country-level growth trends from the data (SM Fig. 11).

We then create a "true" effect of ENSO on growth and attempt to recover it with the DL model. This predetermined ENSO effect is ultimately arbitrary, but we choose country-level effects that are similar in magnitude to the effects we find in our main regression. We set these effects to accumulate over the first 5 years and plateau at that 5-year value permanently. The non-interacted effect of E is set to sum to 3 p.p. per s.d. and the interaction coefficient with τ is set to sum to -6 p.p. per s.d., meaning that a country with $\tau^E = 1.0$ experiences a cumulative effect of -3.0 p.p. per s.d. (3 + 1.0*-6).

We then fit Eqn. 1 using this synthetic growth data and the actual E-index time series and τ^E values, using between 5 and 18 lags in the regression equation (beyond 18 lags, the coefficients become undefined as the degrees of freedom decrease). We repeat this entire process 1,000 times for each number of lags, keeping the set El Niño effect constant. SM Fig. 5 shows the results from these estimations for one example teleconnection value ($\tau^E = 1.0$). Models with between 5 and 10 lags are unbiased, with the central estimate of the coefficient matching the imputed effect. However, the confidence intervals steadily grow as lags are added. With 15 or more lags, the coefficients become biased and statistically insignificant. These results demonstrate that even with a known permanent effect of El Niño, estimating additional lag terms induces sufficient uncertainty to yield biased and insignificant coefficients. To assume that El Niño has no effect in the 15-lag model therefore risks a Type II error.

Economic damages from extreme El Niño events

The regression coefficients derived from Eqn. 1, β and θ, provide estimates of the change in economic growth for a 1-s.d. change in the E-index. These coefficients can then be applied to actual and hypothetical E-index time series to calculate the growth effects of specific historical El Niño events. Here we focus on the two major El Niño events of 1982-83 and 1997-98. We develop "counterfactual" E-index time series wherein these events did not occur by setting the corresponding E-index values (1983 and 1998) to zero. We then apply the regression coefficients to the actual and counterfactual time series to calculate the growth difference between them over the five years after the event. Formally, if E^O represents the observed E-index in the year of the event (*t*), and E^{CF} represents the counterfactual E-index in that year, we calculate the growth change in country *i* from year *t* through year *t*+*L* as:

$$\Delta g_{i(t+L)} = \left[\beta_L E_t^{CF} + \Theta_L E_t^{CF} * \tau_i^E\right] - \left[\beta_L E_t^{O} + \Theta_L E_t^{O} * \tau_i^E\right] \tag{3}$$

We add these growth change values to the observed growth data, yielding a counterfactual growth time series, and we integrate counterfactual growth to calculate counterfactual income from the year of the event to 5 years after the event. Losses due to each event are calculated as the difference between observed and counterfactual income. Details of this procedure can be found in Diffenbaugh and Burke (*73*).

Note that E^{CF} is zero in our analysis, so the first bracketed term on the right-hand-side of Eqn. 3 is zero, but we provide the full equation because it generalizes to other counterfactual E-index values.

The above analysis only incorporates reductions in growth due to the El Niño events. However, because El Niño events can dynamically trigger La Niña events (*34*), which have beneficial effects (SM Fig. 6), a full accounting of the effects of El Niño should incorporate these offsetting beneficial events. The 1982-83 El Niño may have trigged the La Niña of 1984-85 (while the C-index was only -0.08 in 1984, it was -0.96 in 1985), and the 1997-98 El Niño may have triggered the major La Niña of 1999-2000 (the C-index was -2.1 in 1999 and -1.93 in 2000). We incorporate these beneficial effects for both El Niño events by setting the C-index values for the following two years (i.e., 1999 and 2000 in the case of the 1998 El Niño) to zero and calculating the growth difference between the actual and counterfactual C-index time series. The total growth change over the five years following the El Niño event is therefore the reduction due to the El Niño event plus the increase due to the following La Niña events.

For both events, we limit our analysis to countries with continuous GDPpc data since 1982 to ensure that the same countries are included in both calculations. This restriction means that nations with short GDPpc records (e.g., post-Soviet nations like Ukraine) are not included in these calculations.

Climate model selection

Many climate models do not realistically represent the physical processes that drive ENSO (*74*–*76*). To ensure that our projections are physically realistic, we filter the simulations we use based on criteria set out in previous studies (*9*, *36*, *76*). We calculate a parameter known as α from each model, which is the quadratic coefficient on the relationship between the first and second principal components from the EOF analysis used to calculate the E-index and C-index (*76*) (see *ENSO indices*).

The observed value of α is -0.34, indicating a strong nonlinearity in the principal component space and a strong differentiation between eastern Pacific and central Pacific El Niño events. Models which simulate an α value closer to the observed value also more effectively represent the variance and skewness in SST anomalies, as well as the distinct eastern and central Pacific El Niño phases (*9*, *76*). We follow Cai et al. (*9*) in selecting all models with α at least 50% of the observed value, meaning -0.17 or less. SM Tables 4-7 show the total and selected realizations for each experiment. We also test the sensitivity of our results to using only one realization from each model (SM Fig. 9).

Our selection criterion preserves the benefit of a multi-model ensemble, allowing us to sample structural uncertainty in model representation of ENSO as well as initial-condition uncertainty, while incorporating information about model skill (*77*). Treating all simulations in a multi-model ensemble equally has been criticized for assuming that all simulations are independent samples that represent the climate system with equal skill (*78*), especially since CMIP is an ensemble of opportunity rather than a systematic sampling of uncertainty space. Our consideration of model skill provides an ensemble estimate that is likely more accurate than could be achieved without such consideration. Other methods such as bias correction (*79*, *80*) could also improve ensemble skill, but we use the simpler selection criterion based on α given its consistency with the E- and C-indices and its use in the ENSO modeling community.

ENSO amplitude and teleconnections in climate models

We define ENSO amplitude as the standard deviation of the quadratically detrended E-index (*9*, *43*). We calculate each climate model simulation's amplitude in the historical period, which we define as 1940-2019 to parallel the observational data, and in the future, which we define as 2020-2099. The 1940-2019 historical period is chosen so that the historical period is the same length as the future period.

We calculate model-based ENSO teleconnections using the same method as the observations. We perform this calculation separately for the historical and future periods, standardizing and linearly detrending each country's temperature and precipitation time series independently for each period. This method removes mean shifts due to global warming or low-frequency variability and allows us to isolate the interannual signal of ENSO.

Economic damages from changes to ENSO

Calculating economic damages from warming-driven ENSO changes requires a counterfactual world where ENSO evolves without rising temperatures. We calculate the counterfactual ENSO time series for each simulation by re-scaling its future time series to have the amplitude that simulation had in the historical period. For example, if E-index amplitude increases by 20% for a given model realization, we calculate its counterfactual E-index time series by multiplying its future time series by 0.8 (i.e., 0.8 = 1 – 0.2). This method preserves the particular sequence of El Niño and La Niña events in the future, since this sequence is assumed to be unforced (SM Fig. 8) but eliminates the forced change in ENSO amplitude.

We calculate counterfactual ENSO teleconnections with a similar "delta method." For each country in each model, we calculate the change in teleconnection value between the historical and future simulations. We then add this change to each country's observed teleconnection value to implicitly bias-correct the model output. The "counterfactual" teleconnections are thus equal to the observed values and the "future" teleconnections are the observed-plus-change values.

We then calculate the economic effects of changes to ENSO amplitude by comparing the future and counterfactual time series and teleconnections from each model. For each year t between 2020 and

2099, we calculate the growth change from year *t* to year *t+5* as the difference between the future and counterfactual time series and teleconnections:

$$\Delta g_{i(t+L)} = \left[\beta_L E_t^F + \Theta_L E_t^F * \tau_i^F\right] - \left[\beta_L E_t^{CF} + \Theta_L E_t^{CF} * \tau_i^{CF}\right] \quad (4)$$

Here, E^F refers to the future E-index time series and E^{CF} refers to the counterfactual E-index time series. Similarly, τ^F refers to future teleconnections and τ^{CF} refers to counterfactual teleconnections. Δg is negative when changes in ENSO amplitude or teleconnections reduce country-level growth. This calculation yields a growth change time series where each value is the combined effect of the contemporaneous and lagged effects. We then calculate economic growth caused by changes in ENSO by applying these growth change values to the SSP income growth projections and integrating growth to calculate income; the new time series represent the deviations from the SSP baselines caused by changes in ENSO amplitude. Damages are calculated as the difference between this new time series and the SSP baseline. Details of this procedure can be found in Burke et al. (*13*). We perform an analogous calculation using the C-index time series and teleconnections to calculate C-index damages. We note that this procedure calculates counterfactual income as accumulated over the entire 21st century, rather than preceding specific events such as in Fig. 2. This distinction is because these two methods are aimed at answering different questions. In Fig. 2, we are interested in the effects of specific El Niño events, whereas in Fig. 4, we are interested in the accumulated effect of human-caused changes in ENSO over the 21st century.

The cumulative effect of persistent shocks depends on the exact time period over which damages are calculated (*69*), so we test the sensitivity of our results to the start year. Starting the damages calculation in 2015 or 2025 rather than 2020 causes slight variation in damages but does not strongly alter our conclusions (SM Fig. 9e).

We incorporate both amplitude and teleconnection changes in our projections. Holding teleconnections constant reduces both the magnitude and uncertainty of the damage projections, though they remain negative on average and negatively skewed (SM Fig. 9d). Further, a key assumption in these calculations is that the β and θ coefficients remain consistent at a given teleconnection level between the past and future, though individual countries' actual teleconnections may change. This assumption would be violated if societies undertook adaptation measures in response to changes in ENSO amplitude or teleconnections to reduce their sensitivity to ENSO, which is why the need for increased adaptation is a key theme in our results.

Finally, our damages calculations use as many simulations from each model as possible (SM Tables 4-7) to sample both model structural differences and differences in outcomes due to internal climate variability. Using only the first simulation from each model can generate different results; for example, the SSP5-8.5 simulation yields benefits and SSP1-2.6 yields stronger losses. However, we emphasize that—conditional on our model selection criterion—all selected simulations from a given model are physically plausible given the forcing and boundary conditions. Therefore, the results we present in Fig. 4 are a more complete accounting of the possible effects of ENSO changes.

Decomposing contributions to economic damages

Economic damages due to El Niño change in any one simulation are due to the combination of its ENSO amplitude change, teleconnection change, and the particular time series of ENSO it simulates. In order to assess how variation in these three different factors shapes uncertainty in projected ENSO damages, we use a multiple regression model. To do this, we pool all simulations from each scenario into a single regression, and regress cumulative damages onto each model's amplitude change, global mean teleconnection change, and the 2020-2069 sum of its E-index time series, the latter of which proxies the "El Niño-ness" of the model time series. We also interact these time series values with the amplitude and teleconnection changes to allow these latter effects to vary based on the particular sequence of El Niños and La Niñas going forward. This analysis allows to assess the individual effects of forced changes in amplitude and teleconnections while also accounting for the interactive role of the unforced ENSO time series, holding the other factors constant.

The sum of the E-index time series over 2020-2069 measures the degree to which ENSO time series has more El Niños than La Niñas (positive values, as in MIROC-ES2L r6i1p1f2 in Fig. 3c) or more La Niñas than El Niños (negative values, as in CESM2-WACCM r3i1p1f1 in Fig. 3c). Other time periods such as 2020-2049 yield similar results but have slightly weaker explanatory power.

The output of this regression model is shown in SM Table 3. The R^2 in our main specification (column 1) is 0.84, so the factors we include in the regression model explain the majority of inter-simulation and inter-scenario variation in damages. To some extent, this is guaranteed, as amplitude and teleconnections are themselves the inputs into the damages calculation. However, the high goodness-of-fit is nonetheless reassuring that we can summarize inter-simulation variation in damages with these simplified metrics. The remaining unexplained variation may be due to the spatial structure of teleconnection change or temporal variation in the ENSO time series not captured by the 2020-2069 sum.

We estimate several forms of this regression, including removing the E-index time series interactions or interacting amplitude and teleconnection changes together. None provide substantially higher explanatory power than our main specification (SM Table 3).

One key caveat to this analysis is that in the actual damages calculation (Eqn. 4), amplitude and teleconnections are multiplied, not linearly added as in a multiple regression model. This regression approach is therefore a linearization of an underlying multiplicative data generating process. Despite this simplification, it remains a useful interpretive tool to understand the importance of individual factors shaping inter-simulation variation in damages, since the CMIP6 simulations are not a systematic sampling of the space of possible amplitude and teleconnection changes.

Acknowledgements

We thank Dartmouth's Research Computing and the Discovery Cluster for computing resources. We thank the World Climate Research Programme, which, through its Working Group on Coupled Modeling, coordinated and promoted CMIP6. This work was supported by National Science Foundation Graduate Research Fellowship #1840344 to C.W.C. and grants from Dartmouth's Neukom Computational Institute, the Wright Center for the Study of Computation and Just Communities, and the Nelson A. Rockefeller Center to J.S.M.

Competing interests

The authors declare no competing interests.

Author contributions

Both authors designed the analysis. C.W.C. performed the analysis. Both authors interpreted the results and wrote the paper.

Data and code availability

All data and code that support of this study will be made available upon publication at github.com/ccallahan45.

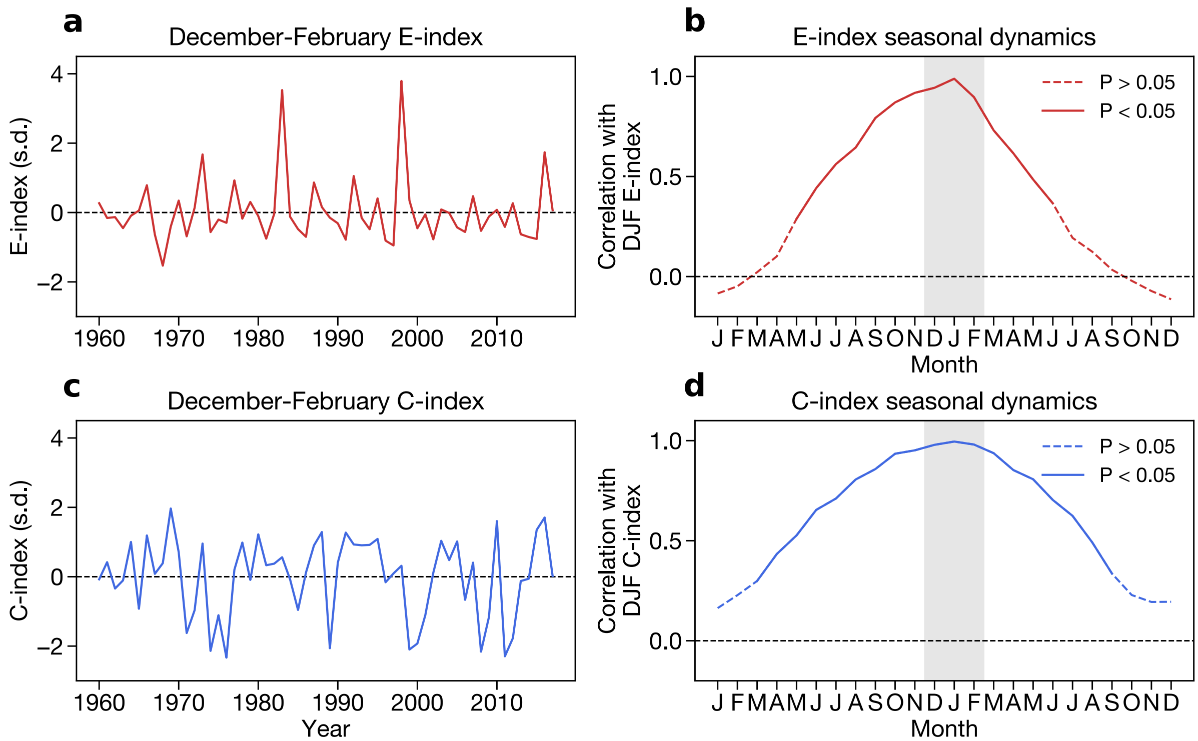

SM Fig. 1 | Interannual and seasonal dynamics of the E- and C-index. A) Timeseries of the average E-index over December, January, and February (DJF) of each year, where the values are referenced to the year of January and February. **B)** Pearson correlation coefficient between the E-index in each month and the DJF-mean E-index. Solid lines denote correlation coefficients that are statistically significant ($p < 0.05$) and dashed lines denote correlation coefficients that are statistically insignificant ($p > 0.05$). **C)** As in (A), but for the DJF C-index. **D)** As in (B), but for the DJF C-index.

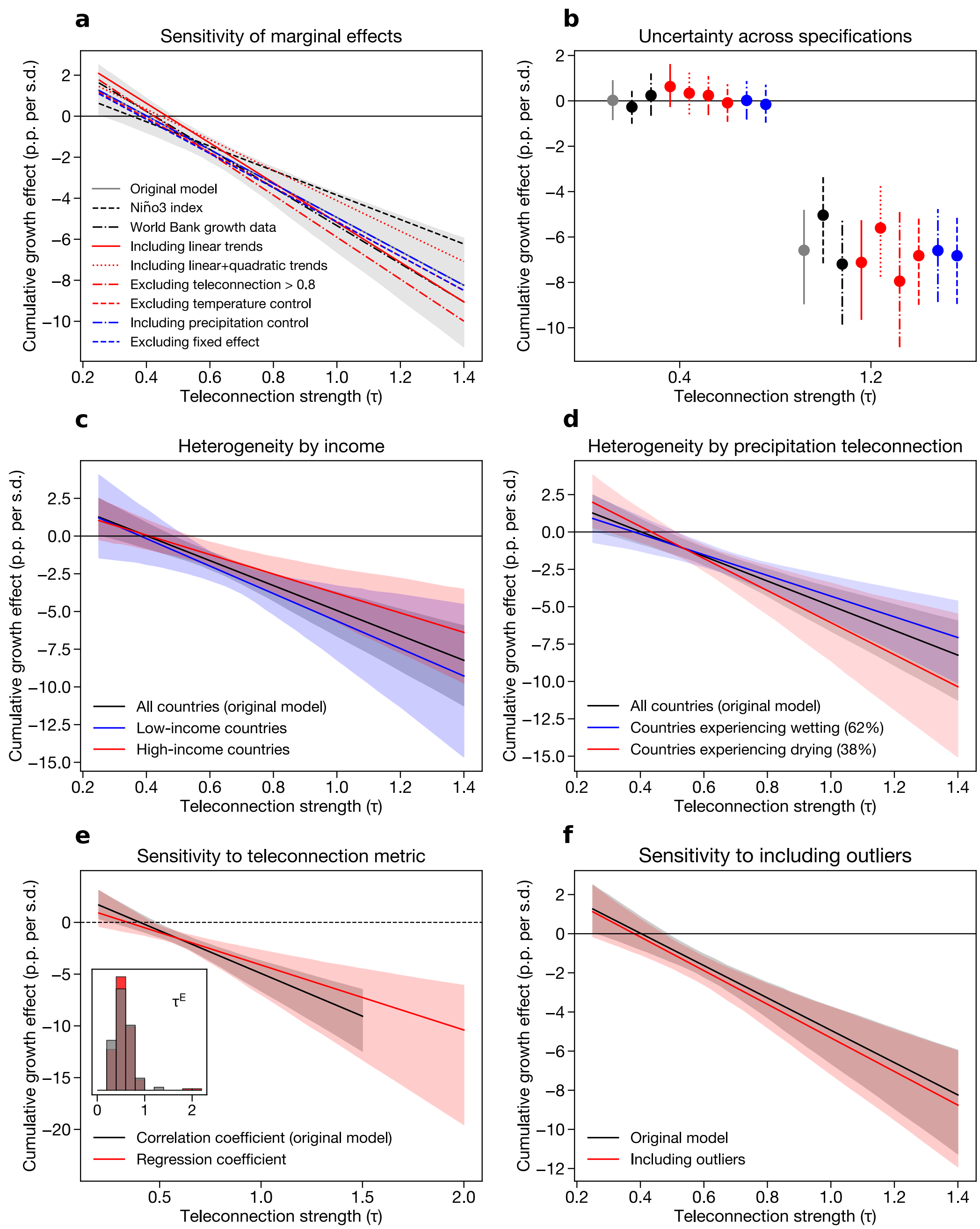

SM Fig. 2 | Sensitivity and heterogeneity of the effect of El Niño. **A)** Cumulative 5-lag effect of El Niño on growth across a range of specifications: the main model (gray line shows mean and shading shows 95% confidence intervals), a model using the Niño3 index instead of the E- and C-index (black dashed line), a model using World Bank growth data instead of the Penn World Tables (black dash-dot line), a model that includes a country-specific linear trend in growth (red solid line), a model that includes both linear and quadratic country-specific trends (red dotted line), a model that excludes countries with teleconnection values greater than 0.8 (red dash-dot line), a model that excludes linear and quadratic temperature controls (red dashed line), a model that includes an annual total precipitation control (blue dash-dot line), and a model that excludes the country fixed effect (blue dashed line). **B)** Uncertainty in the 5-year cumulative marginal effects of El Niño across each model specification at two representative teleconnection values (0.4 and 1.2). Line styles denote alternative models presented in (A). **C)** Cumulative marginal effects of El Niño for low-income countries (blue) and high-income countries (red), as defined by World Bank income classifications (Methods). **D)** Cumulative marginal effects of El Niño for countries experiencing wetting in response to El Niño (positive correlation between the E-index and precipitation, blue) and countries experiencing drying (negative correlation between the E-index and precipitation, red). In (C) and (D), the original model estimated for all countries is shown in black. For each of these samples, we use the original teleconnection value calculated with absolute values in the distributed lag model, but split the sample by the sign of the precipitation teleconnection. **E)** Cumulative marginal effects of El Niño when using the partial correlation coefficient to measure teleconnections (the main analysis) and when using the regression coefficient instead (red). Inset histograms show the distribution of the two teleconnection metrics. **F)** Cumulative marginal effects of El Niño when not including outliers (growth values greater than 0.18 or less than -0.18, black) or when including all values (red). In panels (C), (D), (E), and (F), solid line denotes the average and shading denotes 95% confidence intervals from bootstrap resampling by country (Methods).

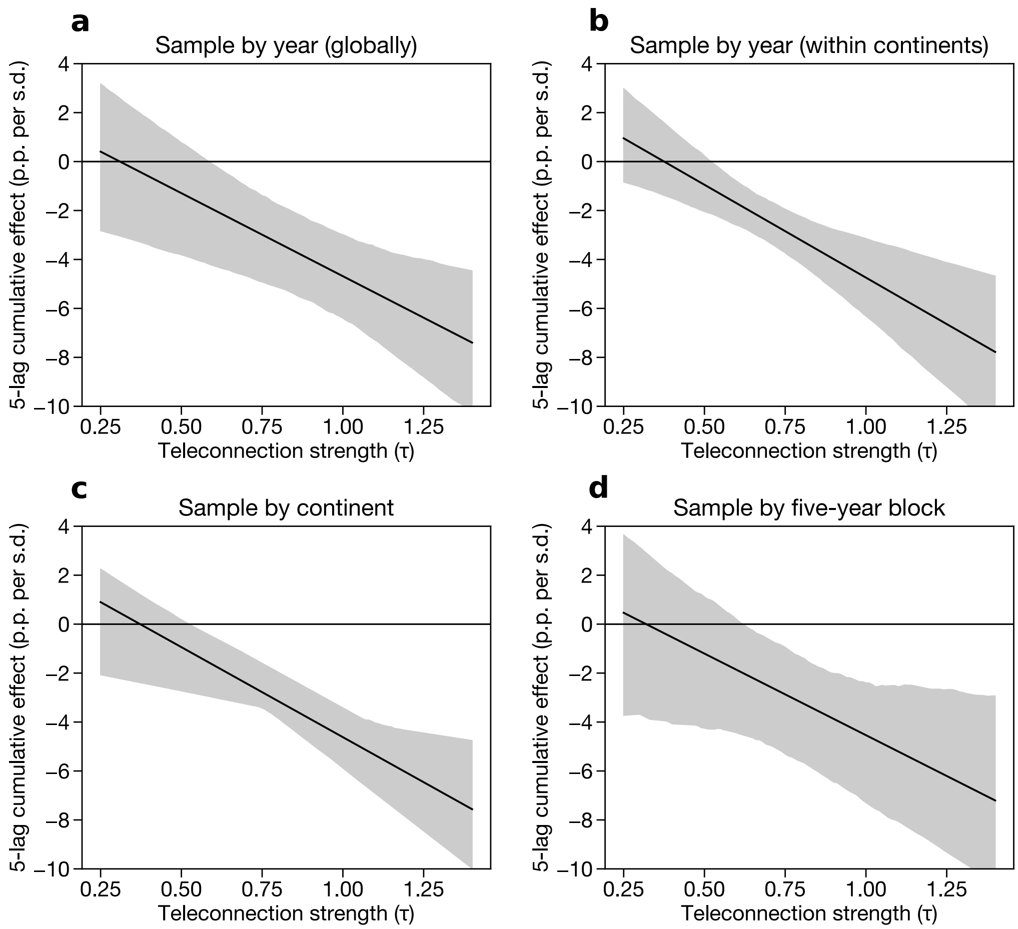

SM Fig. 3 | Regression results using alternative bootstrap sampling schemes. A) Cumulative 5-lag effect of ENSO on economic growth when sampling by year, keeping all countries from a given year together, to account for global spatial correlation in growth within a given year. **B)** Effect when sampling by continent-year combinations to account for spatial correlation in growth within specific continents in a given year. **C)** Effect when sampling by continents to account for simultaneous within-continent temporal and spatial correlation in growth. **D)** Effect when sampling by five-year blocks to account for global spatial correlation in growth and short-term (i.e., five-year) temporal correlation in growth. In all cases, solid line shows the mean and shading shows the 95% confidence intervals. All samples are taken from uniform distributions with replacement. All axes are the same ranges across panels.

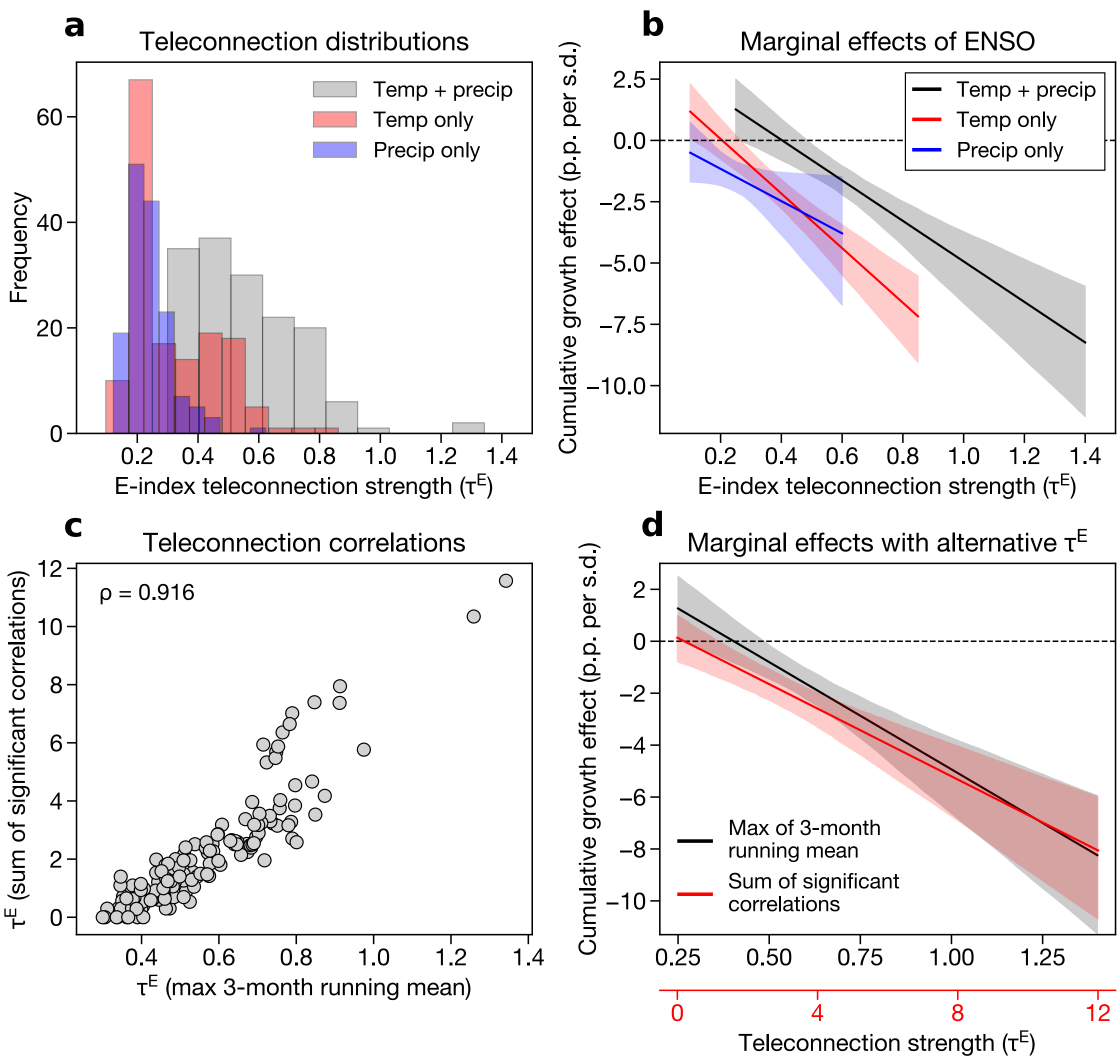

SM Fig. 4 | Comparison of results using alternative teleconnection metrics. A) Distributions of country-level teleconnections using monthly temperature correlation coefficients (red), monthly precipitation correlation coefficients (blue), and their sum (gray). All values are positive since we transform the correlations to absolute values. **B)** Cumulative 5-lag effect of ENSO on economic growth using temperature-only teleconnections (red), precipitation-only teleconnections (blue), and temperature-plus-precipitation teleconnections (black). **C)** Relationship between teleconnections from our main analysis (maximum of three-month running mean) and alternative teleconnections using the sum of all statistically significant correlation coefficients across the months for each country. Rho denotes the Spearman's rank correlation coefficient between the two teleconnection metrics. **D)** Cumulative 5-lag effect of ENSO on economic growth using the original metric (black) and the summed correlation coefficient teleconnection metric (red). In (B) and (D), solid line shows mean and shading shows 95% confidence intervals across 1000 bootstrap iterations, as in the main analysis.

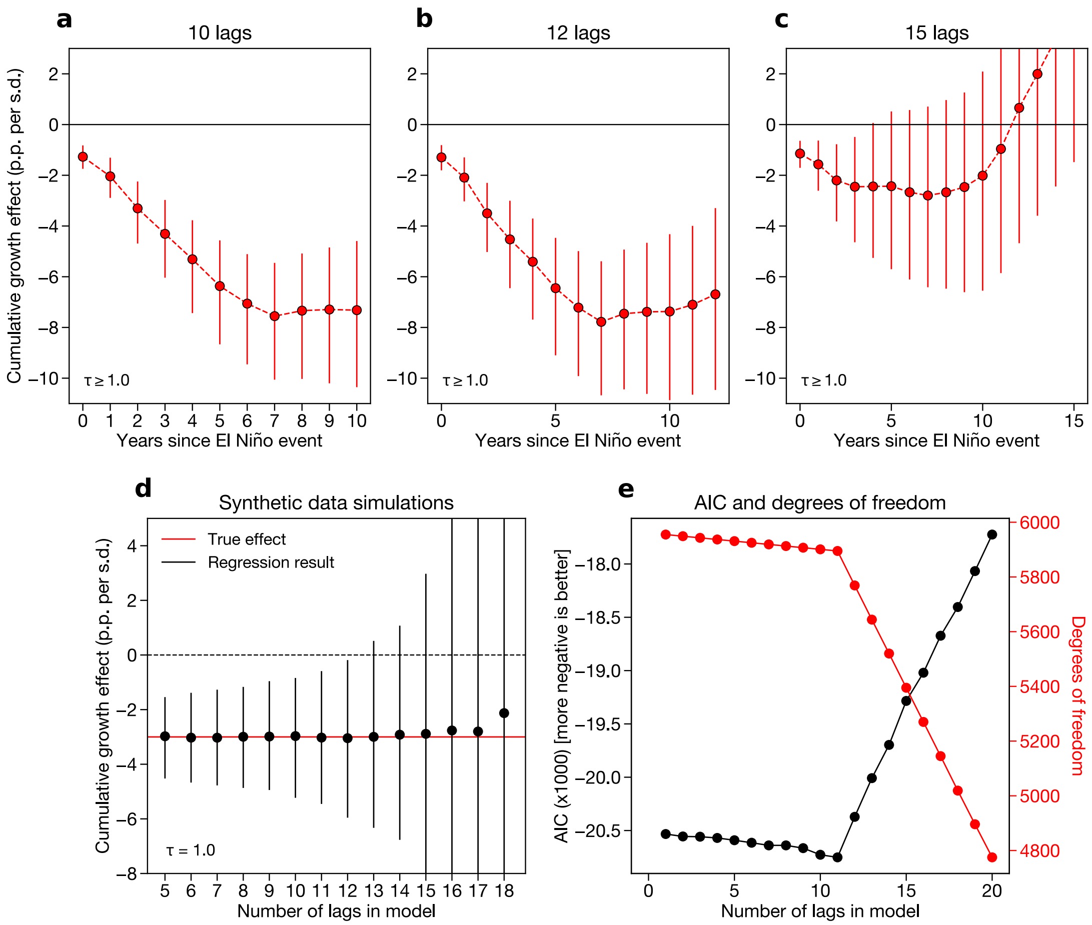

SM Fig. 5 | Sensitivity of main regression results to additional lags. A-C) Regression results for countries with teleconnections greater than or equal to 1.0, estimated with 10 (**A**), 12 (**B**), or 15 (**C**) lags in the regression model. Confidence intervals are estimated by bootstrap resampling as in the main analysis. **D)** Results from synthetic data simulations where a "true" negative ENSO growth effect is imputed to the data and then estimated using models with lags between 5 and 18 (Methods). Coefficients estimated using this perfect model framework are shown for a hypothetical country with $\tau = 1.0$. **E)** Black line shows Akaike Information Criterion (AIC) values for a series of regression models with an increasing number of lags from 1 to 20. More negative AIC values are more desirable. AIC values are divided by 1000 for readability. Red line shows the number of degrees of freedom for the same set of models.

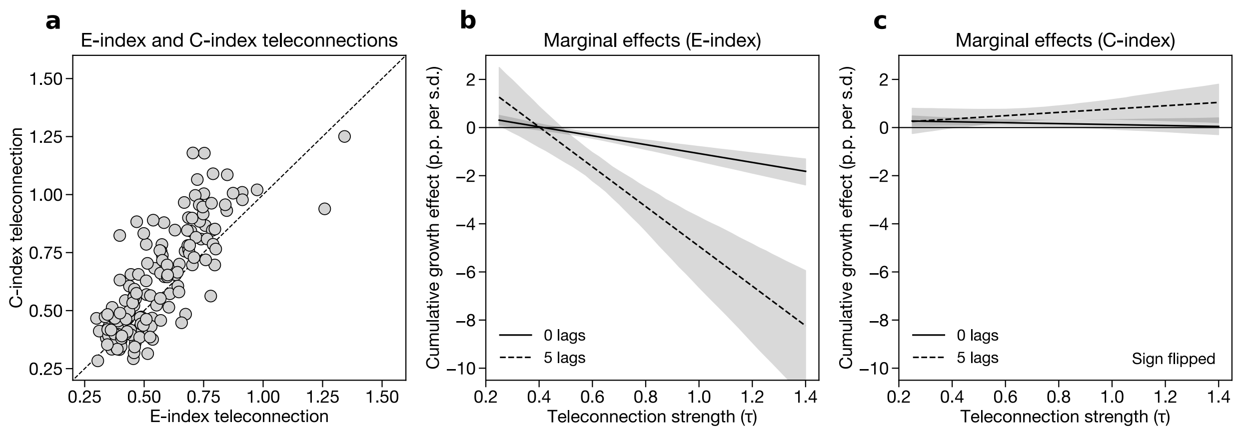

SM Fig. 6 | Teleconnections and marginal effects for both the E-index and C-index. A) Comparison of country-specific teleconnection metrics calculated using the E-index (x-axis) and C-index (y-axis). Dashed line denotes the one-to-one line. **B)** Marginal effects of El Niño (measured by the E-index) at 0 and 5 lags across a range of teleconnection values. **C)** Marginal effects of La Niña (measured by the C-index) at 0 and 5 lags across a range of teleconnection values. The sign on the coefficients in (C) is flipped to measure the effect of moving from 0 to -1 (i.e., moving from a neutral state to a La Niña state). In (B) and (C), effects are calculated from a regression that includes both the E-index and C-index and their corresponding teleconnection metrics (Methods). Lines denote averages and shading denotes 95% confidence intervals using bootstrap resampling by country (Methods).

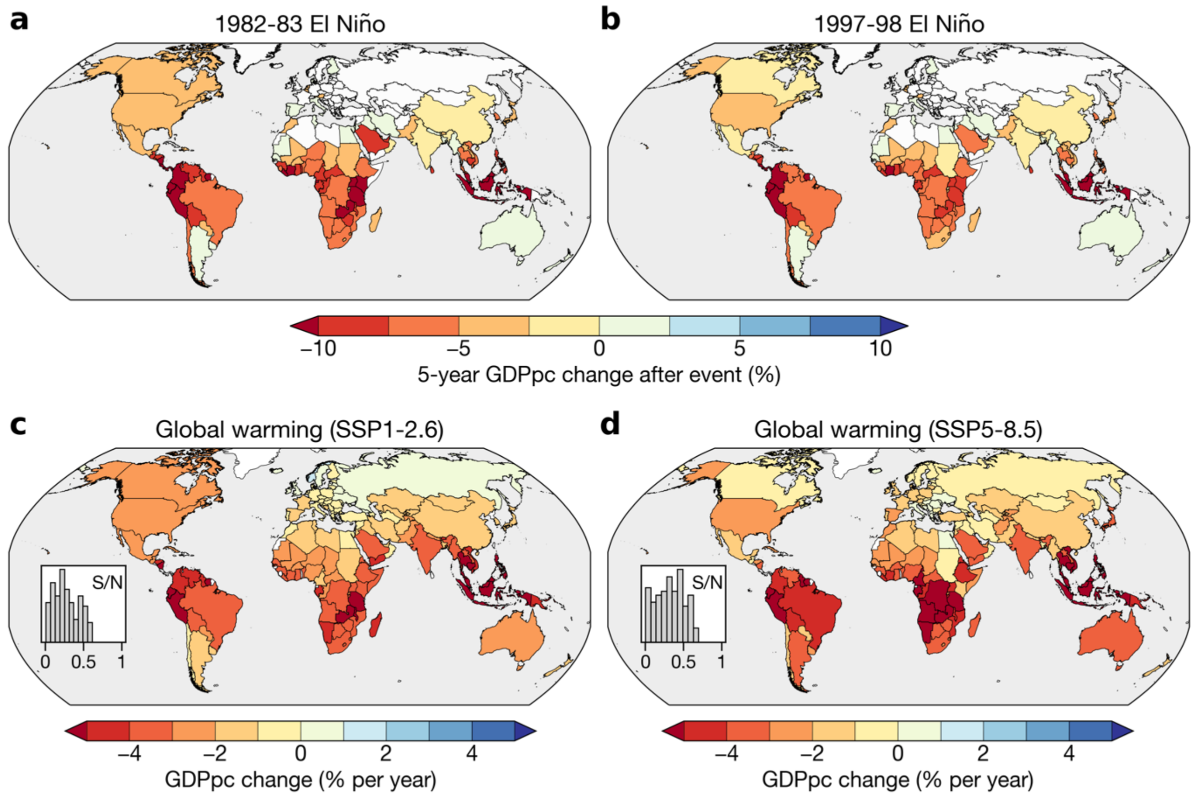

SM Fig. 7 | Country-level losses from extreme El Niño events and global warming. A, B) Change in country-level GDPpc five years after two specific extreme El Niño events: 1982-83 (A) and 1997-98 (B). Changes are calculated relative to counterfactual trajectories in which the event did not occur (see Fig. 3a for example of Peru). That is, the color for Brazil in panel B indicates that Brazil's GDP per capita would have been 5% larger in 2003 if the 1997-98 El Niño event did not occur. Countries are masked in white if they either have no significant marginal effect of ENSO (hatched countries in Fig. 1c) or do not have continuous GDPpc data since 1982 (Methods). **C, D)** 2020-2099 average change in country-level GDPpc under the SSP1-2.6 (C) and SSP5-8.5 (D) scenarios for the average case across climate models and regression bootstraps. Insets in C and D show the signal-to-noise ratios (S/N), meaning the absolute value of the ratio of the ensemble mean GDPpc change to the ensemble standard deviation GDPpc change. "Ensemble" is defined as all possible combinations of climate model projections and regression bootstraps.

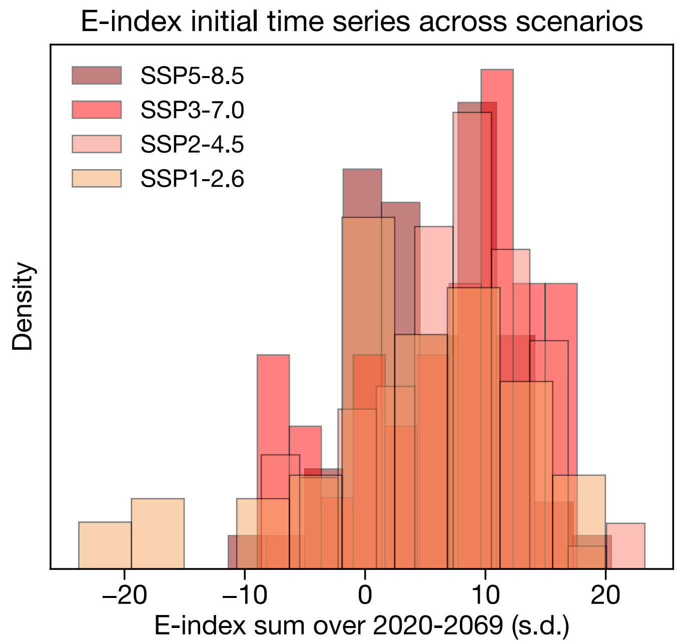

SM Fig. 8 | E-index sum across scenarios. Histograms show the distribution of 2020-2069 E-index sum values across simulations within each SSP scenario. Positive values mean that the simulation's E-index time series has more El Niños than La Niñas.

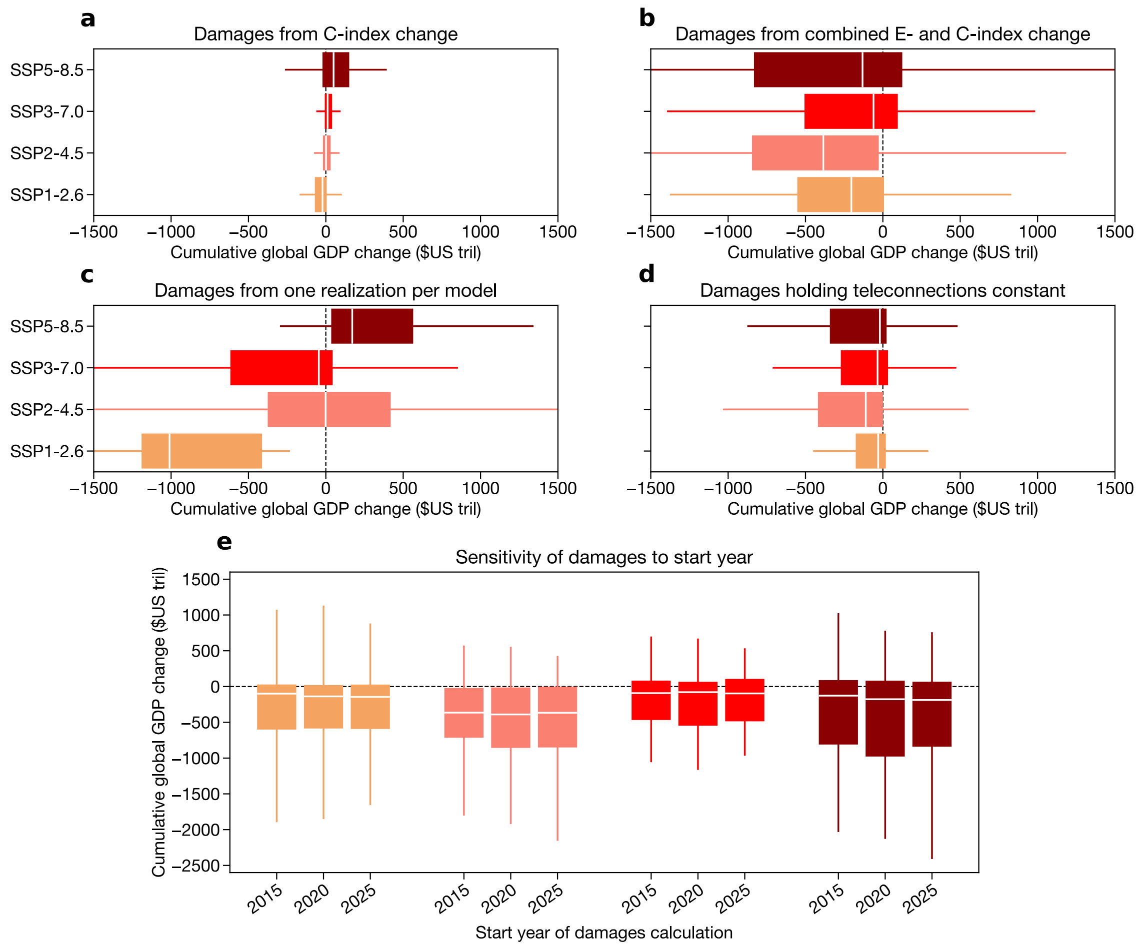

SM Fig. 9 | Sensitivity of damages to alternative choices. As in main text Fig. 4a, but for damages due to changes in C-index amplitude and teleconnections (A), damages due to the combination of changes in E- and C-index amplitude and teleconnections (B), E-index damages using only the first realization from each model (C), E-index damages using amplitude change but holding teleconnections constant (D), and E-index damages when varying the start year of the calculation (E). All panels use a constant 2% discount rate.

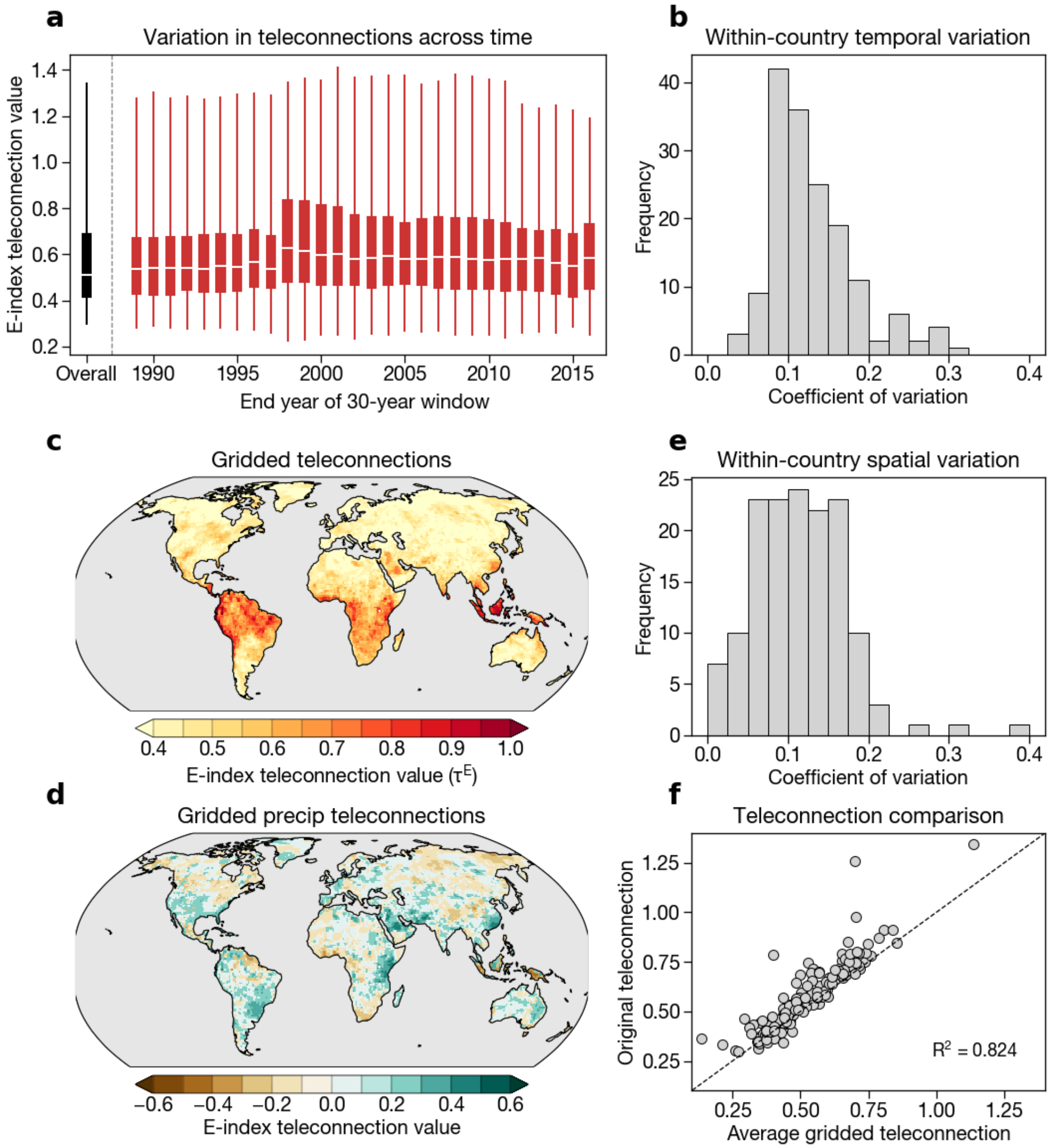

SM Fig. 10 | Spatiotemporal heterogeneity of observed teleconnections. A) Distribution of E-index teleconnections in 30-year windows, with x-axis tick marking the final year of the 30-year window. An end year of 2015, for example, implies a start year of 1986. The black boxplot shows the original distribution of teleconnections calculated over the whole 1960-2016 period. White lines show medians, boxes extend to the 25^{th} and 75^{th} percentiles, and whiskers span the range of the data. **B)** Within-country temporal variation, calculated as the coefficient of variation over the 30-year windows shown in (**A**). This calculation is performed by dividing the standard deviation of each country's teleconnection values over all 30-year windows by its mean teleconnection over those windows. **C)** Grid-cell E-index teleconnections, calculated using the same method as the country-level teleconnections, but with standardized grid-cell temperature and precipitation data. **D)** Grid-cell precipitation teleconnections, meaning the precipitation component of (C). Note that the sign is preserved in (D), whereas the teleconnections in (C) and in the main analysis use absolute values. **E)** Within-country spatial variation in teleconnections, calculated as the coefficient variation of the grid-cell teleconnections when aggregated to the country scale. **F)** Relationship between gridded teleconnections when averaged at the country scale (with population weighting) and the original country-level teleconnections using country-average temperature and precipitation data.

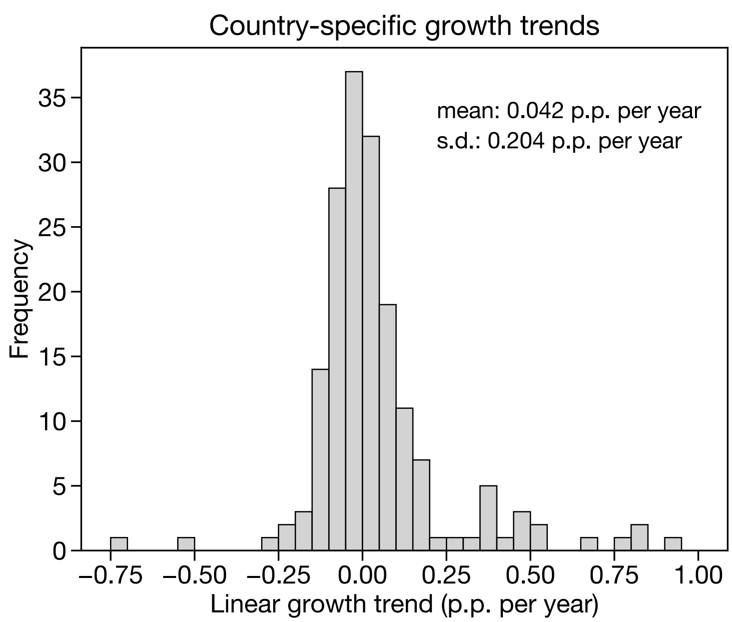

SM Fig. 11 | Linear trends in growth. Growth trends are calculated as the linear coefficient on the univariate regression of each country's growth time series onto time. Only countries with 10 or more years of growth data are included in this histogram. Text in the top right denotes the mean and standard deviation of the distribution of trends across countries.

	Dependent variable: growth				
	(1)	(2)	(3)	(4)	(5)
E_t (β_0)	0.0076***	0.0076*	0.0076*	0.0076*	0.0076*
	(0.0017)	(0.0033)	(0.0036)	(0.0025)	(0.0039)
E_{t-1} (β_1)	0.0029	0.0029	0.0029	0.0029	0.0029
	(0.0021)	(0.0033)	(0.0040)	(0.0024)	(0.0040)
E_{t-2} (β_2)	0.0041	0.0041	0.0041	0.0041	0.0041
	(0.0025)	(0.0049)	(0.0049)	(0.0049)	(0.0045)
E_{t-3} (β_3)	0.0075**	0.0075*	0.0075*	0.0075	0.0075**
	(0.0025)	(0.0037)	(0.0035)	(0.0036)	(0.0027)
E_{t-4} (β_4)	0.0042*	0.0042	0.0042	0.0042	0.0042
	(0.0021)	(0.0036)	(0.0029)	(0.0025)	(0.0025)
E_{t-5} (β_5)	0.0057*	0.0057	0.0057	0.0057*	0.0057
	(0.0023)	(0.0035)	(0.0035)	(0.0019)	(0.0031)
$E_t \times \tau_i^E$ (Θ_0)	−0.0184***	−0.0184**	−0.0184***	−0.0184**	−0.0184**
	(0.0030)	(0.0057)	(0.0047)	(0.0036)	(0.0056)
$E_{t-1} \times \tau_i^E$ (Θ_1)	−0.0097**	−0.0097*	−0.0097	−0.0097**	−0.0097
	(0.0034)	(0.0049)	(0.0055)	(0.0024)	(0.0058)
$E_{t-2} \times \tau_i^E$ (Θ_2)	−0.0142***	−0.0142*	−0.0142*	−0.0142	−0.0142**
	(0.0042)	(0.0067)	(0.0057)	(0.0072)	(0.0048)
$E_{t-3} \times \tau_i^E$ (Θ_3)	−0.0155***	−0.0155**	−0.0155***	−0.0155*	−0.0155***
	(0.0038)	(0.0054)	(0.0037)	(0.0049)	(0.0019)
$E_{t-4} \times \tau_i^E$ (Θ_4)	−0.0109**	−0.0109*	−0.0109***	−0.0109*	−0.0109***
	(0.0036)	(0.0052)	(0.0032)	(0.0031)	(0.0025)
$E_{t-4} \times \tau_i^E$ (Θ_5)	−0.0119**	−0.0119*	−0.0119**	−0.0119***	−0.0119**
	(0.0038)	(0.0055)	(0.0043)	(0.0013)	(0.0042)
Observations	6697	6697	6697	6697	6697
R^2	0.1169	0.1169	0.1169	0.1169	0.1169
Clustering	Country	Year-continent	Year	Continent	Five-year block

$^{***}p < 0.001$; $^{**}p < 0.01$; $^{*}p < 0.05$

SM Table 1 | E-index coefficients with alternative clustering techniques. E-index regression coefficients from the main regression model (Eqn. 1) using various parametric standard error clustering schemes. The marginal effect of the E-index for a country *i* is calculated as the main effect of the E-index plus the interaction term times τ^E_i ($\beta + \theta * \tau^E_i$, main text Eqn. 2). Clustering accounts for both spatiotemporal autocorrelation in errors as well as heteroskedasticity across clusters. In all models, the C-index terms, linear and nonlinear annual mean temperature terms, and the country fixed effect are included but not shown in the table for simplicity.

	Dependent variable: growth				
	(1)	(2)	(3)	(4)	(5)
C_t (Φ_0)	-0.0033^{*}	-0.0033	-0.0033	-0.0033	-0.0033
	(0.0016)	(0.0026)	(0.0031)	(0.0014)	(0.0050)
C_{t-1} (Φ_1)	0.0043^{***}	0.0043	0.0043	0.0043	0.0043
	(0.0012)	(0.0041)	(0.0043)	(0.0019)	(0.0037)
C_{t-2} (Φ_2)	0.0007	0.0007	0.0007	0.0007	0.0007
	(0.0014)	(0.0036)	(0.0042)	(0.0016)	(0.0021)
C_{t-3} (Φ_3)	0.0017	0.0017	0.0017	0.0017	0.0017
	(0.0011)	(0.0031)	(0.0038)	(0.0016)	(0.0031)
C_{t-4} (Φ_4)	-0.0015	-0.0015	-0.0015	-0.0015	-0.0015
	(0.0013)	(0.0035)	(0.0039)	(0.0010)	(0.0019)
C_{t-5} (Φ_5)	-0.0029	-0.0029	-0.0029	-0.0029^{*}	-0.0029
	(0.0015)	(0.0025)	(0.0028)	(0.0009)	(0.0035)
$C_t \times \tau_i^C$ (Ψ_0)	0.0021	0.0021	0.0021	0.0021	0.0021
	(0.0022)	(0.0035)	(0.0037)	(0.0017)	(0.0061)
$C_{t-1} \times \tau_i^C$ (Ψ_1)	-0.0076^{***}	-0.0076	-0.0076	-0.0076^{*}	-0.0076^{*}
	(0.0017)	(0.0051)	(0.0046)	(0.0028)	(0.0036)
$C_{t-2} \times \tau_i^C$ (Ψ_2)	-0.0033	-0.0033	-0.0033	-0.0033	-0.0033
	(0.0020)	(0.0046)	(0.0046)	(0.0025)	(0.0026)
$C_{t-3} \times \tau_i^C$ (Ψ_3)	-0.0012	-0.0012	-0.0012	-0.0012	-0.0012
	(0.0016)	(0.0040)	(0.0042)	(0.0020)	(0.0034)
$C_{t-4} \times \tau_i^C$ (Ψ_4)	0.0011	0.0011	0.0011	0.0011	0.0011
	(0.0019)	(0.0045)	(0.0043)	(0.0011)	(0.0023)
$C_{t-5} \times \tau_i^C$ (Ψ_5)	0.0023	0.0023	0.0023	0.0023^{*}	0.0023
	(0.0021)	(0.0033)	(0.0028)	(0.0006)	(0.0033)
Observations	6697	6697	6697	6697	6697
R^2	0.1169	0.1169	0.1169	0.1169	0.1169
Clustering	Country	Year-continent	Year	Continent	Five-year block

$^{***}p < 0.001$; $^{**}p < 0.01$; $^{*}p < 0.05$

SM Table 2 | C-index coefficients with alternative clustering techniques. C-index regression coefficients from the main regression model (Eqn. 1) using various parametric standard error clustering schemes. The marginal effect of the C-index for a country *i* is calculated as the main effect of the C-index plus the interaction term times τ^C_i ($\phi + \Psi * \tau^C_i$, main text Eqn. 2). Clustering accounts for both spatiotemporal autocorrelation in errors as well as heteroskedasticity across clusters. In all models, the E-index terms, linear and nonlinear annual mean temperature terms, and the country fixed effect are included but not shown in the table for simplicity.

	Dependent variable: Cumulative damages (US$ trillions)			
	(1)	(2)	(3)	(4)
Δ amplitude	-600.46^{***}	-721.75^{*}	-975.1^{**}	-717.46^{***}
	(139.35)	(285.69)	(301.32)	(138.54)
Δ teleconnections	-3145^{***}	-2007.89^{*}	-2904.12^{**}	-3381.96^{***}
	(357.04)	(862.48)	(895.31)	(370.88)
$\sum$E (2020-69)	-1.49	-34.24^{***}		0.32
	(2.86)	(8.67)		(3.01)
$\sum$E (2020-69) $\times$ Δ amplitude	-69.2^{**}			-77.69^{***}
	(20.9)			(20.65)
$\sum$E (2020-69) $\times$ Δ teleconnections	-531^{***}			-540.23^{***}
	(49.11)			(55.41)
Δ amplitude $\times$ Δ teleconnections				2090.52
				(1479.12)
Observations	239	239	239	239
Adjusted R^2	0.838	0.418	0.281	0.839

$^{***}p < 0.001$; $^{**}p < 0.01$; $^{*}p < 0.05$

SM Table 3 | Effects of ENSO amplitude change, teleconnection change, and time series realization on global economic output. Each column shows the coefficients from a regression analysis with each simulation's cumulative discounted global GDP change as the dependent variable. "Δ amplitude" refers to each simulation's E-index amplitude change, "Δ teleconnections" refers to each simulation's global mean teleconnection change, and "ΣE (2020-69)" refers to the sum of each simulation's E-index time series over 2020-2069 to capture whether the time series contains more El Niños or La Niñas. 2020-2069 is used because it has the highest explanatory power relative to other potential periods, but many alternatives such as 2020-2049 yield broadly similar results. Model data are pooled across all SSP scenarios. Amplitude and teleconnection values are in their native units, but the E-index sum is centered so that zero corresponds to the mean E-index time series realizations. Therefore, the amplitude and teleconnection coefficients can be interpreted as *the change in global GDP due to amplitude or teleconnection changes given the average time series realization*. Standard errors are HC3 heteroskedasticity-robust standard errors.

Model	Total realizations	Selected realizations
CanESM5	50	0
KACE-1-0-G	3	0
MIROC-ES2L	7	7
MIROC6	50	50
MRI-ESM2-0	5	4

SM Table 4 | CMIP6 models and realizations used from the SSP1-2.6 scenario. Monthly sea surface temperature (“tos”), monthly atmospheric temperature (“tas”), and daily precipitation (“pr”) are used from each model. Bolded models are those that have at least 1 realization selected for the final analysis (Methods).

Model	Total realizations	Selected realizations
ACCESS-CM2	3	0
ACCESS-ESM1-5	11	0
CAMS-CSM1-0	1	0
CESM2	2	0
CESM2-WACCM	3	2
CMCC-CM2-SR5	1	1
CMCC-ESM2	1	1
CNRM-CM6-1	1	0
CanESM5	50	0
EC-Earth3	8	8
FGOALS-g3	3	0
GFDL-ESM4	1	0
HadGEM3-GC31-LL	1	0
INM-CM4-8	1	0
INM-CM5-0	1	0
IPSL-CM6A-LR	5	0
KACE-1-0-G	3	0
MIROC-ES2L	30	30
MIROC6	33	33
MPI-ESM1-2-HR	2	1
MPI-ESM1-2-LR	10	9
NorESM2-LM	2	0
NorESM2-MM	2	1
UKESM1-0-LL	5	0

SM Table 5 | CMIP6 models and realizations used from the SSP2-4.5 scenario. Monthly sea surface temperature (“tos”), monthly atmospheric temperature (“tas”), and daily precipitation (“pr”) are used from each model. Bolded models are those that have at least 1 realization selected for the final analysis (Methods).

Model	Total realizations	Selected realizations
ACCESS-CM2	3	0
ACCESS-ESM1-5	10	0
CAMS-CSM1-0	1	0
CESM2	2	0
CESM2-WACCM	1	1
CMCC-CM2-SR5	1	1
CMCC-ESM2	1	1
CNRM-CM6-1	1	0
CanESM5	50	0
FGOALS-g3	4	0
GFDL-ESM4	1	0
INM-CM4-8	1	0
INM-CM5-0	5	0
IPSL-CM6A-LR	5	0
KACE-1-0-G	3	0
MIROC-ES2L	10	10
MIROC6	3	3
MPI-ESM1-2-HR	10	4
MPI-ESM1-2-LR	7	6
MRI-ESM2-0	5	5
NorESM2-LM	1	1
NorESM2-MM	1	1
UKESM1-0-LL	13	0

SM Table 6 | CMIP6 models and realizations used from the SSP3-7.0 scenario. Monthly sea surface temperature (“tos”), monthly atmospheric temperature (“tas”), and daily precipitation (“pr”) are used from each model. Bolded models are those that have at least 1 realization selected for the final analysis (Methods).

Model	Total realizations	Selected realizations
ACCESS-CM2	2	0
ACCESS-ESM1-5	6	0
CAMS-CSM1-0	1	0
CESM2	0	0
CESM2-WACCM	3	1
CMCC-CM2-SR5	1	1
CMCC-ESM2	1	1
CNRM-CM6-1	1	0
CanESM5	50	0
FGOALS-g3	3	0
GFDL-ESM4	1	0
HadGEM3-GC31-LL	4	0
HadGEM3-GC31-MM	4	0
INM-CM4-8	1	0
INM-CM5-0	1	0
IPSL-CM6A-LR	4	0
KACE-1-0-G	3	0
MIROC-ES2L	1	1
MIROC6	50	50
MPI-ESM1-2-HR	2	1
NorESM2-LM	1	1
NorESM2-MM	1	1
UKESM1-0-LL	5	0

SM Table 7 | CMIP6 models and realizations used from the SSP5-8.5 scenario. Monthly sea surface temperature (“tos”), monthly atmospheric temperature (“tas”), and daily precipitation (“pr”) are used from each model. Bolded models are those that have at least 1 realization selected for the final analysis (Methods).

	E_t	E_{t-1}	E_{t-2}	E_{t-3}	E_{t-4}	E_{t-5}
E_t		-0.01	-0.299	-0.022	0.026	-0.016
E_{t-1}			-0.074	-0.283	0.002	0.016
E_{t-2}				-0.085	-0.294	0.004
E_{t-3}					-0.096	-0.293
E_{t-4}						-0.094

SM Table 8 | Correlation matrix for the E-index and its lags. Each table entry shows the Pearson correlation coefficient between the E-index at various time lags and the E-index at each other time lag.

References

1. M. J. McPhaden, S. E. Zebiak, M. H. Glantz, ENSO as an Integrating Concept in Earth Science. *Science*. **314**, 1740–1745 (2006).

2. J. Bjerknes, ATMOSPHERIC TELECONNECTIONS FROM THE EQUATORIAL PACIFIC. *Mon. Weather Rev.* **97**, 163–172 (1969).

3. S.-W. Yeh, W. Cai, S.-K. Min, M. J. McPhaden, D. Dommenget, B. Dewitte, M. Collins, K. Ashok, S.-I. An, B.-Y. Yim, J.-S. Kug, ENSO Atmospheric Teleconnections and Their Response to Greenhouse Gas Forcing. *Rev. Geophys.* **56**, 185–206 (2018).

4. T. W. Corringham, D. R. Cayan, The Effect of El Niño on Flood Damages in the Western United States. *Weather Clim. Soc.* **11**, 489–504 (2019).

5. F. J. Magilligan, P. S. Goldstein, El Niño floods and culture change: A late Holocene flood history for the Rio Moquegua, southern Peru. *Geology*. **29**, 431–434 (2001).

6. S. M. Hsiang, K. C. Meng, Tropical Economics. *Am. Econ. Rev.* **105**, 257–261 (2015).

7. T. Iizumi, J.-J. Luo, A. J. Challinor, G. Sakurai, M. Yokozawa, H. Sakuma, M. E. Brown, T. Yamagata, Impacts of El Niño Southern Oscillation on the global yields of major crops. *Nat. Commun.* **5**, 3712 (2014).

8. S. M. Hsiang, K. C. Meng, M. A. Cane, Civil conflicts are associated with the global climate. *Nature*. **476**, 438–441 (2011).

9. W. Cai, G. Wang, B. Dewitte, L. Wu, A. Santoso, K. Takahashi, Y. Yang, A. Carréric, M. J. McPhaden, Increased variability of eastern Pacific El Niño under greenhouse warming. *Nature*. **564**, 201–206 (2018).

10. W. Cai, B. Ng, G. Wang, A. Santoso, L. Wu, K. Yang, Increased ENSO sea surface temperature variability under four IPCC emission scenarios. *Nat. Clim. Change*, 1–4 (2022).

11. W. Cai, S. Borlace, M. Lengaigne, P. van Rensch, M. Collins, G. Vecchi, A. Timmermann, A. Santoso, M. J. McPhaden, L. Wu, M. H. England, G. Wang, E. Guilyardi, F.-F. Jin, Increasing frequency of extreme El Niño events due to greenhouse warming. *Nat. Clim. Change*. **4**, 111–116 (2014).

12. W. Cai, A. Santoso, M. Collins, B. Dewitte, C. Karamperidou, J.-S. Kug, M. Lengaigne, M. J. McPhaden, M. F. Stuecker, A. S. Taschetto, A. Timmermann, L. Wu, S.-W. Yeh, G. Wang, B. Ng, F. Jia, Y. Yang, J. Ying, X.-T. Zheng, T. Bayr, J. R. Brown, A. Capotondi, K. M. Cobb, B. Gan, T. Geng, Y.-G. Ham, F.-F. Jin, H.-S. Jo, X. Li, X. Lin, S. McGregor, J.-H. Park, K. Stein, K. Yang, L. Zhang, W. Zhong, Changing El Niño–Southern Oscillation in a warming climate. *Nat. Rev. Earth Environ.* **2**, 628–644 (2021).

13. M. Burke, S. M. Hsiang, E. Miguel, Global non-linear effect of temperature on economic production. *Nature*. **527**, 235–239 (2015).

14. M. Burke, V. Tanutama, Climatic constraints on aggregate economic output. *Natl. Bur. Econ. Res. Work. Pap.* (2019).

15. M. Dell, B. F. Jones, B. A. Olken, Temperature shocks and economic growth: Evidence from the last half century. *Am. Econ. J. Macroecon.* **4**, 66–95 (2012).

16. M. Letta, R. S. J. Tol, Weather, Climate and Total Factor Productivity. *Environ. Resour. Econ.* **73**, 283–305 (2019).

17. M. Kalkuhl, L. Wenz, The impact of climate conditions on economic production. Evidence from a global panel of regions. *J. Environ. Econ. Manag.* **103**, 102360 (2020).

18. M. Kotz, A. Levermann, L. Wenz, The effect of rainfall changes on economic production. *Nature*. **601**, 223–227 (2022).

19. M. Kotz, L. Wenz, A. Stechemesser, M. Kalkuhl, A. Levermann, Day-to-day temperature variability reduces economic growth. *Nat. Clim. Change*, 1–7 (2021).

20. P. Cashin, K. Mohaddes, M. Raissi, Fair weather or foul? The macroeconomic effects of El Niño. *J. Int. Econ.* **106**, 37–54 (2017).

21. S. C. Smith, D. Ubilava, The El Niño Southern Oscillation and Economic Growth in the Developing World. *Glob. Environ. Change*. **45**, 151–164 (2017).

22. R. Generoso, C. Couharde, O. Damette, K. Mohaddes, The Growth Effects of El Niño and La Niña: Local Weather Conditions Matter. *Ann. Econ. Stat.*, 83–126 (2020).

23. A. D. Brunner, El Niño and World Primary Commodity Prices: Warm Water or Hot Air? *Rev. Econ. Stat.* **84**, 176–183 (2002).

24. D. Ubilava, El Niño, La Niña, and world coffee price dynamics. *Agric. Econ.* **43**, 17–26 (2012).

25. D. Ubilava, The ENSO Effect and Asymmetries in Wheat Price Dynamics. *World Dev.* **96**, 490–502 (2017).

26. F. C. Moore, D. B. Diaz, Temperature impacts on economic growth warrant stringent mitigation policy. *Nat. Clim. Change*. **5**, 127 (2015).

27. E. J. Moyer, M. D. Woolley, N. J. Matteson, M. J. Glotter, D. A. Weisbach, Climate impacts on economic growth as drivers of uncertainty in the social cost of carbon. *J. Leg. Stud.* **43**, 401–425 (2014).

28. S. Dietz, N. Stern, Endogenous growth, convexity of damage and climate risk: how Nordhaus' framework supports deep cuts in carbon emissions. *Econ. J.* **125**, 574–620 (2015).

29. K. Takahashi, A. Montecinos, K. Goubanova, B. Dewitte, ENSO regimes: Reinterpreting the canonical and Modoki El Niño. *Geophys. Res. Lett.* **38** (2011).

30. E. M. Rasmusson, T. H. Carpenter, Variations in Tropical Sea Surface Temperature and Surface Wind Fields Associated with the Southern Oscillation/El Niño. *Mon. Weather Rev.* **110**, 354–384 (1982).

31. D. Ubilava, M. Abdolrahimi, The El Niño impact on maize yields is amplified in lower income teleconnected countries. *Environ. Res. Lett.* **14**, 054008 (2019).

32. S. Power, M. Haylock, R. Colman, X. Wang, The Predictability of Interdecadal Changes in ENSO Activity and ENSO Teleconnections. *J. Clim.* **19**, 4755–4771 (2006).

33. N. S. Diffenbaugh, F. V. Davenport, M. Burke, Historical warming has increased U.S. crop insurance losses. *Environ. Res. Lett.* **16**, 084025 (2021).

34. W. Cai, G. Wang, A. Santoso, M. J. McPhaden, L. Wu, F.-F. Jin, A. Timmermann, M. Collins, G. Vecchi, M. Lengaigne, M. H. England, D. Dommenget, K. Takahashi, E. Guilyardi, Increased frequency of extreme La Niña events under greenhouse warming. *Nat. Clim. Change*. **5**, 132–137 (2015).

35. van Aalst, M.K., Fankhauser, S., Kane, S.M., Sponberg, K., Climate information and forecasting for development: lessons from the 1997/98 El Niño (2000).

36. W. Cai, B. Ng, T. Geng, L. Wu, A. Santoso, M. J. McPhaden, Butterfly effect and a self-modulating El Niño response to global warming. *Nature*. **585**, 68–73 (2020).

37. N. Maher, D. Matei, S. Milinski, J. Marotzke, ENSO change in climate projections: forced response or internal variability? *Geophys. Res. Lett.* **45**, 11–390 (2018).

38. C. Deser, R. Knutti, S. Solomon, A. S. Phillips, Communication of the role of natural variability in future North American climate. *Nat. Clim. Change*. **2**, 775–779 (2012).

39. K.-S. Yun, J.-Y. Lee, A. Timmermann, K. Stein, M. F. Stuecker, J. C. Fyfe, E.-S. Chung, Increasing ENSO–rainfall variability due to changes in future tropical temperature–rainfall relationship. *Commun. Earth Environ.* **2**, 1–7 (2021).

40. K. Hu, G. Huang, P. Huang, Y. Kosaka, S.-P. Xie, Intensification of El Niño-induced atmospheric anomalies under greenhouse warming. *Nat. Geosci.* **14**, 377–382 (2021).

41. R. Seager, N. Naik, L. Vogel, Does Global Warming Cause Intensified Interannual Hydroclimate Variability? *J. Clim.* **25**, 3355–3372 (2012).

42. A. T. Wittenberg, A. Rosati, T. L. Delworth, G. A. Vecchi, F. Zeng, ENSO Modulation: Is It Decadally Predictable? *J. Clim.* **27**, 2667–2681 (2014).

43. C. W. Callahan, C. Chen, M. Rugenstein, J. Bloch-Johnson, S. Yang, E. J. Moyer, Robust decrease in El Niño/Southern Oscillation amplitude under long-term warming. *Nat. Clim. Change*. **11**, 752–757 (2021).

44. Council of Economic Advisers, Discounting for public policy: Theory and recent evidence on the merits of updating the discount rate (2017), (available at https://obamawhitehouse.archives.gov/sites/default/files/page/files/201701_cea_discounting_issue_brief.pdf).

45. M. Meinshausen, J. Lewis, C. McGlade, J. Gütschow, Z. Nicholls, R. Burdon, L. Cozzi, B. Hackmann, Realization of Paris Agreement pledges may limit warming just below 2 °C. *Nature*. **604**, 304–309 (2022).

46. B. O'Neill, M. van Aalst, Z. Zaiton Ibrahim, L. Berrang Ford, S. Bhadwal, H. Buhaug, D. Diaz, K. Frieler, M. Garschagen, A. Magnan, G. Midgely, A. Mirzabaev, A. Thomas, R. Warren, "Key Risks

Across Sectors and Regions" in *Climate Change 2022: Impacts, Adaptation and Vulnerability. Contribution of Working Group II to the Sixth Assessment Report of the Intergovernmental Panel on Climate Change* (Cambridge University Press, Cambridge, UK and New York, NY, USA), pp. 2411–2538.

47. A. French, R. Mechler, "Managing El Niño risks under uncertainty in Peru" (International Institute for Applied Systems Analysis, 2017), (available at https://pure.iiasa.ac.at/id/eprint/14849/1/French_Mechler_2017_El%20Ni%c3%b1o_Risk_Peru_Report.pdf).

48. B. Huang, P. W. Thorne, V. F. Banzon, T. Boyer, G. Chepurin, J. H. Lawrimore, M. J. Menne, T. M. Smith, R. S. Vose, H.-M. Zhang, Extended Reconstructed Sea Surface Temperature, Version 5 (ERSSTv5): Upgrades, Validations, and Intercomparisons. *J. Clim.* **30**, 8179–8205 (2017).

49. N. A. Rayner, D. E. Parker, E. B. Horton, C. K. Folland, L. V. Alexander, D. P. Rowell, E. C. Kent, A. Kaplan, Global analyses of sea surface temperature, sea ice, and night marine air temperature since the late nineteenth century. *J. Geophys. Res. Atmospheres*. **108** (2003), doi:10.1029/2002JD002670.

50. R. A. Rohde, Z. Hausfather, The Berkeley Earth Land/Ocean Temperature Record. *Earth Syst. Sci. Data Discuss.*, 1–16 (2020).

51. C. J. Willmott, Terrestrial air temperature and precipitation: Monthly and annual time series (1950-1996). *WWW Url Httpclimate Geog Udel Edu∼Clim. Ghcnts Html* (2000).

52. G. P. Compo, J. S. Whitaker, P. D. Sardeshmukh, N. Matsui, R. J. Allan, X. Yin, B. E. Gleason, R. S. Vose, G. Rutledge, P. Bessemoulin, others, The twentieth century reanalysis project. *Q. J. R. Meteorol. Soc.* **137**, 1–28 (2011).

53. U. Schneider, A. Becker, P. Finger, A. Meyer-Christoffer, B. Rudolf, M. Ziese, GPCC full data reanalysis version 6.0 at 0.5: monthly land-surface precipitation from rain-gauges built on GTS-based and historic data. *GPCC Data Rep Doi*. **10** (2011).

54. M. Auffhammer, S. M. Hsiang, W. Schlenker, A. Sobel, Using weather data and climate model output in economic analyses of climate change. *Rev. Environ. Econ. Policy*. **7**, 181–198 (2013).

55. A. R. Gottlieb, J. S. Mankin, Observing, Measuring, and Assessing the Consequences of Snow Drought. *Bull. Am. Meteorol. Soc.* **1** (2021), doi:10.1175/BAMS-D-20-0243.1.

56. C. W. Callahan, J. S. Mankin, National attribution of historical climate damages. *Clim. Change*. **172**, 40 (2022).

57. C. U. Center for International Earth Science Information Network CIESIN, *Gridded Population of the World, Version 4 (GPWv4): Population Count* (2016).

58. R. C. Feenstra, R. Inklaar, M. P. Timmer, The next generation of the Penn World Table. *Am. Econ. Rev.* **105**, 3150–82 (2015).

59. A. Deaton, A. Heston, Understanding PPPs and PPP-Based National Accounts. *Am. Econ. J. Macroecon.* **2**, 1–35 (2010).

60. T. W. Bank, *World Development Indicators 2016* (2016).

61. V. Eyring, S. Bony, G. A. Meehl, C. A. Senior, B. Stevens, R. J. Stouffer, K. E. Taylor, Overview of the Coupled Model Intercomparison Project Phase 6 (CMIP6) experimental design and organization. *Geosci. Model Dev.* **9**, 1937–1958 (2016).

62. B. C. O'Neill, C. Tebaldi, D. P. van Vuuren, V. Eyring, P. Friedlingstein, G. Hurtt, R. Knutti, E. Kriegler, J.-F. Lamarque, J. Lowe, G. A. Meehl, R. Moss, K. Riahi, B. M. Sanderson, The Scenario Model Intercomparison Project (ScenarioMIP) for CMIP6. *Geosci. Model Dev.* **9**, 3461–3482 (2016).

63. C. Tebaldi, K. Debeire, V. Eyring, E. Fischer, J. Fyfe, P. Friedlingstein, R. Knutti, J. Lowe, B. O'Neill, B. Sanderson, D. van Vuuren, K. Riahi, M. Meinshausen, Z. Nicholls, K. B. Tokarska, G. Hurtt, E. Kriegler, J.-F. Lamarque, G. Meehl, R. Moss, S. E. Bauer, O. Boucher, V. Brovkin, Y.-H. Byun, M. Dix, S. Gualdi, H. Guo, J. G. John, S. Kharin, Y. Kim, T. Koshiro, L. Ma, D. Olivié, S. Panickal, F. Qiao, X. Rong, N. Rosenbloom, M. Schupfner, R. Séférian, A. Sellar, T. Semmler, X. Shi, Z. Song, C. Steger, R. Stouffer, N. Swart, K. Tachiiri, Q. Tang, H. Tatebe, A. Voldoire, E. Volodin, K. Wyser, X. Xin, S. Yang, Y. Yu, T. Ziehn, Climate model projections from the Scenario Model Intercomparison Project (ScenarioMIP) of CMIP6. *Earth Syst. Dyn.* **12**, 253–293 (2021).

64. S. Hoyer, J. Hamman, xarray: N-D labeled arrays and datasets in Python. *J Open Res Softw. Revis.* (2017).

65. F. Jia, W. Cai, B. Gan, L. Wu, E. Di Lorenzo, Enhanced North Pacific impact on El Niño/Southern Oscillation under greenhouse warming. *Nat. Clim. Change*, 1–8 (2021).

66. B. Ng, W. Cai, T. Cowan, D. Bi, Impacts of Low-Frequency Internal Climate Variability and Greenhouse Warming on El Niño–Southern Oscillation. *J. Clim.* **34**, 2205–2218 (2021).

67. E. Tziperman, M. A. Cane, S. E. Zebiak, Y. Xue, B. Blumenthal, Locking of El Niño's Peak Time to the End of the Calendar Year in the Delayed Oscillator Picture of ENSO. *J. Clim.* **11**, 2191–2199 (1998).

68. M. Newman, P. D. Sardeshmukh, Are we near the predictability limit of tropical Indo-Pacific sea surface temperatures? *Geophys. Res. Lett.* **44**, 8520–8529 (2017).

69. M. Burke, W. M. Davis, N. S. Diffenbaugh, Large potential reduction in economic damages under UN mitigation targets. *Nature*. **557** (2018).

70. S. M. Hsiang, A. S. Jina, The causal effect of environmental catastrophe on long-run economic growth: Evidence from 6,700 cyclones. *Natl. Bur. Econ. Res. Work. Pap.* (2014).

71. S. Hsiang, Climate econometrics. *Annu. Rev. Resour. Econ.* **8**, 43–75 (2016).

72. J. H. Stock, M. W. Watson, Vector Autoregressions. *J. Econ. Perspect.* **15**, 101–115 (2001).

73. N. S. Diffenbaugh, M. Burke, Global warming has increased global economic inequality. *Proc. Natl. Acad. Sci.* **116**, 9808–9813 (2019).

74. E. Guilyardi, A. Wittenberg, A. Fedorov, M. Collins, C. Wang, A. Capotondi, G. J. van Oldenborgh, T. Stockdale, Understanding El Niño in Ocean–Atmosphere General Circulation Models: Progress and Challenges. *Bull. Am. Meteorol. Soc.* **90**, 325–340 (2009).

75. R. Seager, M. Cane, N. Henderson, D.-E. Lee, R. Abernathey, H. Zhang, Strengthening tropical Pacific zonal sea surface temperature gradient consistent with rising greenhouse gases. *Nat. Clim. Change*. **9**, 517–522 (2019).

76. C. Karamperidou, F.-F. Jin, J. L. Conroy, The importance of ENSO nonlinearities in tropical pacific response to external forcing. *Clim. Dyn.* **49**, 2695–2704 (2017).

77. R. Knutti, J. Sedláček, B. M. Sanderson, R. Lorenz, E. M. Fischer, V. Eyring, A climate model projection weighting scheme accounting for performance and interdependence. *Geophys. Res. Lett.* **44**, 1909–1918 (2017).

78. R. Knutti, The end of model democracy? *Clim. Change*. **102**, 395–404 (2010).

79. P. Huang, J. Ying, A Multimodel Ensemble Pattern Regression Method to Correct the Tropical Pacific SST Change Patterns under Global Warming. *J. Clim.* **28**, 4706–4723 (2015).

80. D. Chen, M. A. Cane, S. E. Zebiak, R. Cañizares, A. Kaplan, Bias correction of an ocean-atmosphere coupled model. *Geophys. Res. Lett.* **27**, 2585–2588 (2000).